RESEARCH PAPER

Optimization method on brace arrangement of center brace steel frame structural system

Yunyun Zhu[1] · Yanjing Fan[1] · Jianrong Pan[1,2] · Fangxin Hu[1,2] · Zhoupeng Wu[1] · Zhan Wang[1,2]

Abstract

Traditional center brace steel frame structural systems typically focus on refining the member cross-section size in the brace arrangement and optimization analysis. However, they often overlook the critical aspects of brace location and overall structural performance that are inherently interconnected. This study highlights the impact of different brace arrangement locations on the structural performance. Consequently, by employing the fundamental principle of maximum structural stiffness and a derived theoretical model of a simplified optimized arrangement, we proposed a novel method for optimizing the arrangement of center braces. This resulted in significant enhancements in the mechanical properties of the steel frame brace structural system compared with traditional approaches. It elucidated the intrinsic connection between the positional parameters of the center brace and the lateral resistance performance of each story and derived a theoretical formula validated through 190 ABAQUS finite element analysis models. Building on this foundation, this study further analyzed the factors influencing the lateral resistance performance within the frame brace system. A simplified mechanical model of the center brace steel frame structure was established, along with an explanation of the brace optimization principles using the basic brace unit. The static and dynamic performances of structures featuring optimal brace arrangements were thoroughly examined to understand their impact on the overall lateral performance and yielding mechanisms. Additionally, the dynamic response of the structures following the implementation of optimal brace arrangements was studied to explore the relationship between brace location and seismic performance.

Keywords Center brace · Steel frame · Brace optimization arrangement · Optimization method · Seismic response

1 Introduction

The capacity to withstand lateral loads has become increasingly critical in the design of tall steel structures (Thai et al. 2020a, 2020b; Fang and Linzell 2021; Lim et al. 2020; Chen et al. 2020; Kontoni and Farghaly 2023). Designers commonly integrate a brace into a frame structure to establish an effective system to resist lateral forces, ensure stability, and enhance the horizontal force resistance (Zheng et al. 2023).

✉ Jianrong Pan
ctjrpan@scut.edu.cn

1 School of Civil Engineering and Transportation, South China University of Technology, Guangzhou 510640, China

2 State Key Laboratory of Subtropical Building and Urban Science, South China University of Technology, Guangzhou 510640, China

Therefore, the brace arrangement significantly influences the structural performance and is vital for ensuring stability and safety (Hongjia et al. 2018). Currently, many designers of steel frame brace structures rely on past experience rather than a strong theoretical foundation for determining the optimal brace layout. This often results in inefficient and economically unfavorable designs, among other problems. Consequently, it is essential to explore efficient and rational methods to optimize brace arrangements in steel structures. This effort aimed to achieve high-performance structural designs and foster sustainable development in structural engineering (Nie et al. 2016; Mourhatch and Krishnan 2022; Zhang et al. 2022).

Exploring the relationship between brace arrangement and overall structural performance is now a pivotal aspect of performance-based design for steel frame brace systems (Gray et al. 2017). The development of an economical, rational, and effective brace layout is of utmost importance (Rahgozar et al. 2017). Consequently, it has become a

central research focus, with the brace arrangement location carrying more weight than the number of braces (Mohammadi et al. 2015). Simultaneously, systematic research on the center brace steel frame structural system, including the optimization of brace arrangement and exploration of principles governing optimal brace placement, holds immense significance for advancing steel frame brace systems.

Numerous studies have investigated the impact of different brace arrangements on the lateral, seismic, and collapse resistances of structures. Yu et al. explored the effects of braces in the horizontal and vertical directions at various locations on the lateral stiffness of the structure. They analyzed 244 brace arrangements to identify those with the highest and lowest lateral stiffnesses. The study revealed that the X- and double-inverted V-type brace arrangements exhibited the highest structural stiffness (Xiaoye et al. 2015). Türker et al. conducted tests to compare the dynamic characteristics of pure steel frame models with brace steel frame models. The results demonstrated that brace arrangement increased the inherent frequency of the structure (Türker and Bayraktar 2013). Tan et al. discussed the key parameters affecting the collapse resistance of center brace steel frame structures and offered suggestions for brace arrangement locations (Tan et al. 2022). Additionally, Tan et al. integrated beam and column members into a continuous topology optimization process for brace frames to obtain an optimal topological configuration (Stromberg et al. 2022). Aydin et al. performed discrete topology optimization of center brace steel frame structures to obtain a topologically optimal brace frame structure with robust collapse resistance (Hassanzadeh and Gholizadeh 2019). Fu et al. optimized the brace position design of steel frame brace structural systems to develop an effective brace arrangement scheme (Bochao et al. 2022).

Existing studies on centrally braced steel frame structural systems have primarily focused on comparing various brace arrangement schemes. However, these investigations have not distinctly explored the differences between brace location parameters and structural performance, nor have they established a universal theory for brace optimization. To address these gaps, this study analyzed the correlation between brace position parameters and the structural performance of center-braced steel frame systems. This elucidated the influence of these parameters on structural performance, which was a pivotal factor in the efficacy of center-braced steel frame structures. In addition, we introduced an optimization method for the center brace arrangement and examined the static and dynamic structural performance following the implementation of this optimized arrangement in steel frames. The technological research roadmap delineates the trajectory of this study depicted in Fig. 1. The following sections outline the specific content and innovative aspects of this study.

(1) A comprehensive theoretical analysis was developed to clarify the relationship between the lateral resistance in steel frame brace structures and their brace arrangement. Additionally, a simplified mechanical model was proposed to optimize the center brace arrangement in steel frames.
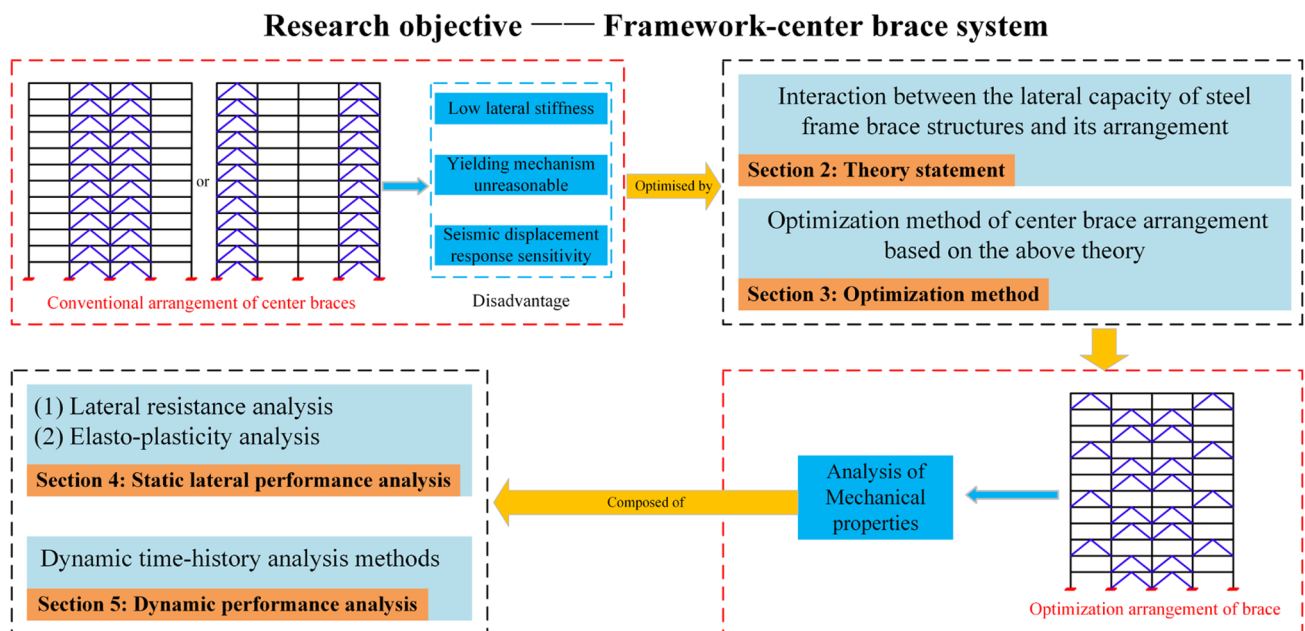

Fig. 1 Technology research roadmap in this paper

(2) According to the theoretical foundation of the simplified mechanical model for optimizing the center brace arrangement, we constructed a quantitative model for the basic brace unit force transmission path. This facilitated the determination of the optimal scheme for center brace optimization and clarified the rules governing the center brace arrangement. These principles constituted the core concept of the steel frame center brace optimization method outlined in this paper.

(3) An extensive series of simulation experiments was conducted to explore both the static and dynamic aspects of the structural behavior subsequent to the implementation of the optimal brace arrangement. This study investigated the effect of the optimized arrangement of braces on the lateral performance and yielding mechanism of the structure, as well as its dynamic response, and analyzed the relationship between the brace positioning and seismic performance of the structure.

2 Optimized theory for center brace arrangement

This study focused on a typical herringbone center brace steel frame structure and investigated how the positioning of brace arrangements affects the lateral resistance on both the ground and general floors. The effects of single-, double-, and multi-span brace arrangements on the lateral stiffness of these areas were also assessed. A theoretical model was established to clarify how multi-span brace arrangements influence the lateral stiffness of structural floors and derive a corresponding theoretical calculation formula.

2.1 Calculation of lateral stiffness for components resisting lateral forces

(1) The lateral stiffness of the herringbone brace (Wang et al. 2022).

The lateral stiffness k_{br} of the herringbone brace (Fig. 2) is

$$k_{br} = \frac{2EA_{br}\text{Cos}^2\theta}{L} = \frac{2EA_{br}\text{Cos}^2\theta\text{Sin}\theta}{h}, \tag{1}$$
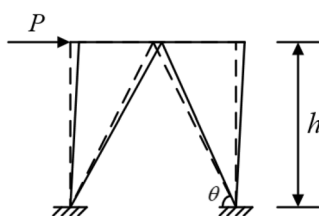

Fig. 2 Calculation diagram of lateral stiffness of herringbone brace

where $(EA)_{br}$ represents the brace tensile and compressive stiffness, h represents the floor height, and θ represents the angle between the herringbone brace and horizontal line.

(2) Lateral stiffness of frame column.

The lateral stiffness K_F of the frame is obtained using the D-value method.

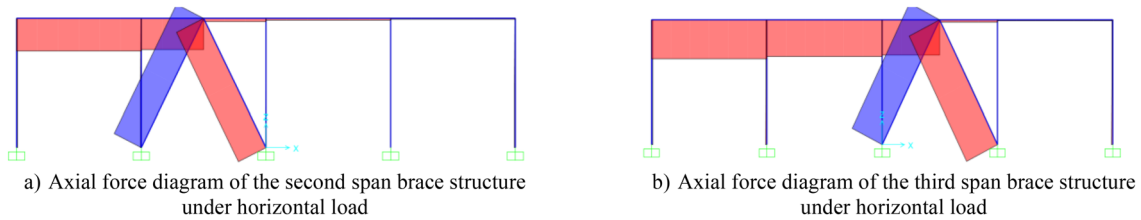$$\begin{cases} K_F = \sum_{i=1}^{n} k_i \\ k_i = \alpha\dfrac{12EI_c}{h^3} \end{cases}, \tag{2}$$

where k_i represents the lateral stiffness of the i-th column, EI_c represents the column flexural stiffness, and α represents the column stiffness correction factor, which can be calculated from the linear stiffness ratio of the beam–column.

2.2 Influence of single-span brace arrangement locations on the lateral resistance performance of structural floors

(1) Simplified analysis model of single-span arrangement of braces.

When subjected to horizontal loads, the brace and beam preceding it could bear most of the load. Prior to the yielding of the brace, transferring the horizontal load to the beam following the brace was challenging, as illustrated in Fig. 3. Therefore, the axial deformation of all frame beams was considered before the brace was reached. Conversely, it is assumed that the axial deformation of the beams after the brace can be neglected. The analysis presented in Fig. 4 illustrates a single-span analysis of an m-span within an n-span subgrade brace. The parameter "m" is introduced to account for the influence of the brace's location on the lateral stiffness of the subfloor.

The axial deformation of the frame beams after the brace was disregarded, and the frame-following brace could be regarded as a unified entity. Considering the relatively small horizontal force exerted by an individual frame column, it was assumed that the axial force on the frame beams preceding the brace node was uniform. To simplify the member connections, the frame columns preceding the brace are grouped into substructure 1, the brace constitutes substructure 2, and the frame after the brace is treated as substructure 3. The corresponding stiffness values are denoted as K_{s1}, K_{s2}, and K_{s3}, respectively. In this study, we considered the axial deformation of all the frame beams up to the brace arrangement position. The axial stiffness of the beams is denoted as K_b. The calculation framework is illustrated in Fig. 5, which neglects the influence of the superstructure. The lateral stiffness values of substructures 1, 2, and 3 were determined using Eq. (3).

a) Axial force diagram of the second span brace structure under horizontal load

b) Axial force diagram of the third span brace structure under horizontal load

Fig. 3 Axial force diagram of single-span brace structure under horizontal load. **a** Axial force diagram of the second span brace structure under horizontal load. **b** Axial force diagram of the third span brace structure under horizontal load
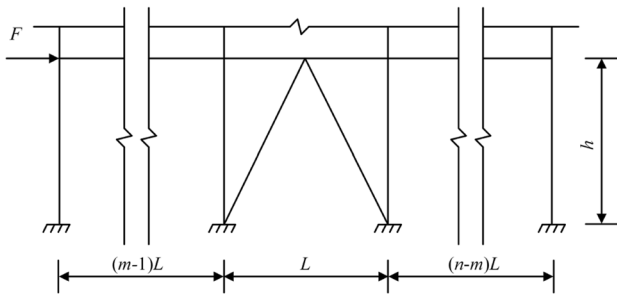
Fig. 4 The m-span arrangement diagram of n-span bottom steel frame brace
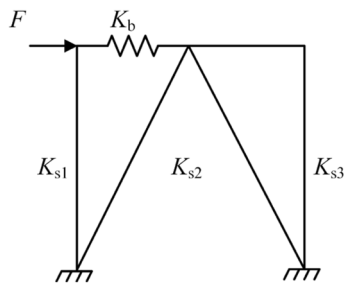
Fig. 5 Substructure calculation diagram

$$\begin{cases} K_{s1} = \sum_{i=1}^{m} k_i \\ K_{s2} = k_{br} \\ K_{s3} = \sum_{i=m+1}^{n+1} k_i \end{cases} \tag{3}$$

Fig. 6 Bottom-brace single-span arrangement deformation diagram

The axial stiffness of the beam was $K_b = EA/L_m$ and $L_m = (m-1)L + 0.5L$, where EA represents the tensile and compressive stiffness of the beam, L_m represents the total beam length considering the axial deformation of the beam, L represents the single-span length of the frame, k_i represents the lateral stiffness of the i-th subfloor column, and k_{br} represents the lateral stiffness of the brace.

(2) The effect of single-span brace arrangement on the lateral stiffness of the bottom floor.

Given the omission of axial deformation in the frame beams after the brace and the incorporation of axial deformation in the beams before the brace, we can partition the total deformation of the overall structural layer into two constituent elements: the axial deformation of the beams (Δ_1) and the deformation of the frame brace (Δ_2), as depicted in Fig. 6. An assessment of the horizontal forces sustained by the substructure is presented in terms of the force considerations, as illustrated in Fig. 7.
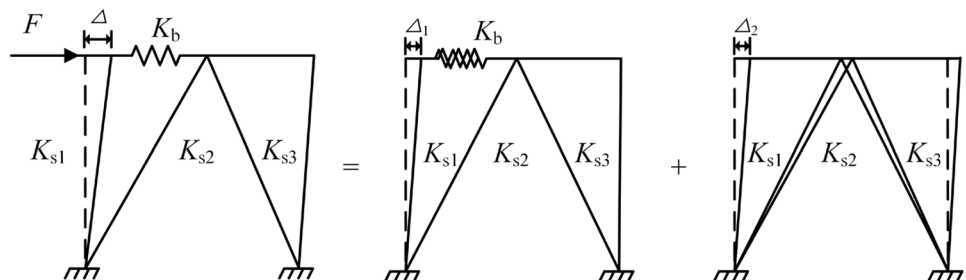
The total deformation of the structural layer and the horizontal forces braced by substructures 1, 2, and 3 are given by Eq. (4).

$$\begin{cases} \Delta = \Delta_1 + \Delta_2 \\ F_1 = K_{s1}(\Delta_1 + \Delta_2) \\ F_2 = K_{s2}\Delta_2 \\ F_3 = K_{s3}\Delta_2 \end{cases} \tag{4}$$

An equilibrium equation for the overall structural force is established $\sum F = 0$.

$$F = F_1 + F_2 + F_3 = K_{s1}\Delta + K_{s2}\Delta_2 + K_{s3}\Delta_2 \tag{5}$$

Fig. 7 Force analysis diagram

Fig. 8 The m-span arrangement diagram of n-span general steel frame brace
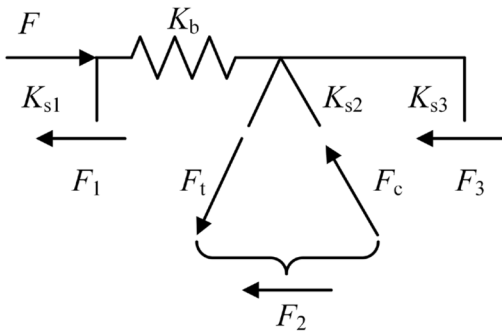
The axial force F_A of the beam, considering axial deformation, can be expressed as follows:

$$F_A = F - F_1 = K_b \Delta_1. \tag{6}$$

Combining Eqs. (4), (5), and (6), we derive

$$F = \frac{K_{s1} + K_{s2} + K_{s3} + K_{s1}(K_{s2} + K_{s3})/K_b}{1 + (K_{s2} + K_{s3})/K_b} \Delta. \tag{7}$$

Because $K = F/\Delta$, the equivalent stiffness at the frame level is

$$
\begin{aligned}
K &= \frac{K_{s1} + K_{s2} + K_{s3} + K_{s1}(K_{s2} + K_{s3})/K_b}{1 + (K_{s2} + K_{s3})/K_b} \\
&= K_{s1} \frac{1}{1/(K_{s2} + K_{s3}) + 1/K_b},
\end{aligned} \tag{8}
$$

where K_{s1}, K_{s2}, and K_{s3} represent the lateral stiffnesses of substructures 1, 2, and 3, respectively, considering the single-span arrangement of the bottom brace, and K_b represents the axial stiffness of the deformed beam.

(3) The effect of single-span brace arrangement on the lateral stiffness of the general floor.

It was varied from the bottom single-span layout by modifying the boundaries of the columns, as shown in Fig. 8. Both the center and side columns should account for the linear stiffness of the connected beams, whereas the bottom ends of the columns were articulated, as illustrated in Fig. 9. It is imperative to emphasize that the subsequent brace in the multi-span arrangement of the general layer adheres to consistent boundary equivalence principles. The lateral stiffness of these columns was corrected using the D-value method to accommodate the variable-stiffness characteristics of the columns on the general floor. This correction facilitates the determination of the equivalent lateral stiffness of the structural floor, which can be obtained using Eq. (9).
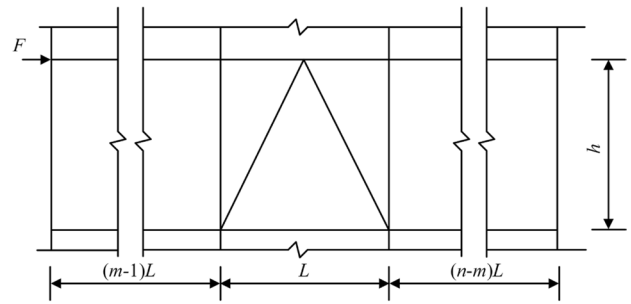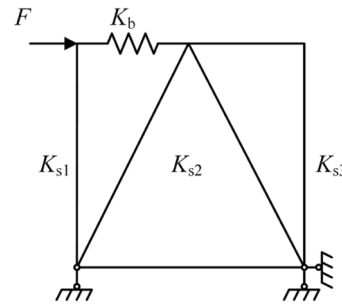

Fig. 9 Substructure calculation diagram

$$
\begin{aligned}
K &= \frac{K_{s1} + K_{s2} + K_{s3} + K_{s1}(K_{s2} + K_{s3})/K_b}{1 + (K_{s2} + K_{s3})/K_b} \\
&= K_{s1} \frac{1}{1/(K_{s2} + K_{s3}) + 1/K_b},
\end{aligned} \tag{9}
$$

where $K_{s1} = \sum_{i=1}^{m} k_i'$, $K_{s2} = k_{br}$, $K_{s3} = \sum_{i=m+1}^{n+1} k_i'$, $K_b = EA/L_m$, $L_m = (m-1)L + 0.5L$, K_b represents the axial stiffness of the deformed beam, EA represents the tensile and compressive stiffness of the beam, L_m denotes the length of the beam taking into account the axial deformation of the beam, L denotes the single-span span, and k_i' represents the lateral stiffness of the i-th general story column, and k_{br} represents the lateral stiffness of the brace.

2.3 Influence of double-span brace random arrangement locations on the lateral resistance performance of structural floors

(1) Simplified analysis model for double-span random arrangement of braces.

For a double-span brace arrangement, varying degrees of axial beam deformation must be considered based on the brace placement, as shown in Fig. 10. Analyzing the double-span arrangement with n-span at the bottom involved

Fig. 10 Axial force diagram of double-span random arrangement structure under a horizontal load
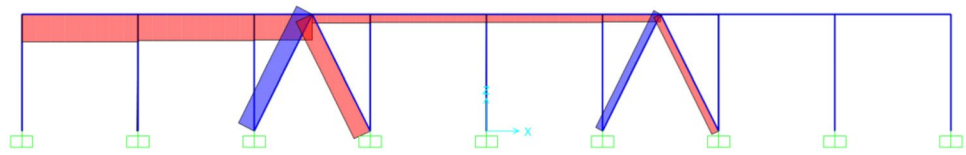
introducing brace position parameters a and b, as depicted in Fig. 11.

The structural layer was divided into four distinct substructures to account for the axial deformation of the various beams, with each division defined by brace nodes as boundaries. Substructure 1 comprises all frame columns positioned prior to the initial span brace node. The stiffness of the frame columns between the braces was evenly divided on both sides of the braces, with the first span brace designated as substructure 2. Substructure 3 corresponds to the second span brace, and any subsequent frames are grouped under substructure 4. Notably, this analysis did not consider the influence of the superstructure. A schematic representation of the substructure calculation is shown in Fig. 12.

(2) The effect of random double-span brace arrangements on the lateral stiffness of the bottom floor.

The lateral stiffness values of substructures 1, 2, 3, and 4 are given by Eq. (10).

$$\begin{cases} K_{s1} = \sum_{i=1}^{a} k_i \\ K_{s2} = k_{br} + 0.5 \sum_{i=a+1}^{b} k_i \\ K_{s3} = k_{br} + 0.5 \sum_{i=a+1}^{b} k_i \\ K_{s4} = \sum_{i=b}^{n+1} k_i \end{cases}, \tag{10}$$

where k_i is the lateral stiffness of the i-th bottom column and k_{br} is the brace lateral stiffness.

When considering substructures 2, 3, and 4 as a whole, the equivalent stiffness is

$$K_{s234} = K_{s2} + \frac{1}{1/(K_{s3} + K_{s4}) + 1/K_{b2}}. \tag{11}$$

Fig. 11 Random arrangement of n-span bottom steel frame brace a and b spans
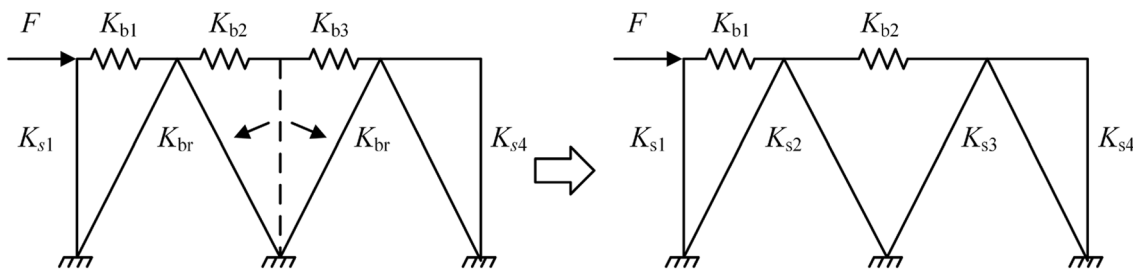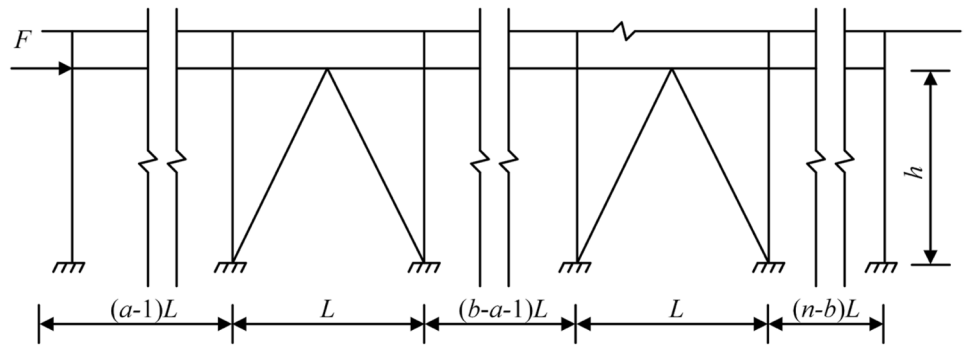
Fig. 12 Random arrangement calculation diagram of n-span bottom steel frame brace a and b spans

The overall lateral stiffness of the structure is determined through a series–parallel combination of individual stiffness components.

$$K = K_{s1} + \frac{1}{1/K_{s234} + 1/K_{b1}} = K_{s1} \frac{1}{\frac{1}{K_{s2}+1/[1/(K_{s3}+K_{s4})+1/K_{b2}]+\frac{1}{K_{b1}}}},$$
(12)

where $K_{b1} = EA/L_a$, $L_a = (a\text{-}1)L + 0.5L$, $K_{b2} = EA/L_b$, and $L_b = (b\text{-}a)L$. K_{b1} and K_{b2} represent the axial linear stiffness of the deformed beam; EA represents the tensile and compressive stiffness of the beam; L_a and L_b denote the total length of the beam considering axial deformation; and L denotes the length of single-span.

(3) The effect of random double-span brace arrangements on the lateral stiffness of the general floor.

The difference primarily involves alterations in the column boundaries between the general story brace double-span random arrangement and the bottom-story brace double-span random arrangement, as depicted in Figs. 13 and 14. To accommodate these changes and account for the modified stiffness correction coefficients, Eq. (13) was used to calculate the stiffness of a steel frame story with a continuous arrangement of a general story brace double-span.

$$K = K_{s1} + \frac{1}{1/K_{s234} + 1/K_{b1}} = K_{s1} + \frac{1}{\frac{1}{K_{s2}+1/[1/(K_{s3}+K_{s4})+1/K_{b2}]} + \frac{1}{K_{b1}}},$$
(13)

where $K_{s1} = \sum_{i=1}^{a} k_i'$, $K_{s2} = k_{br} + 0.5\sum_{i=a+1}^{b} k_i'$, $K_{s3} = k_{br} + 0.5\sum_{i=a+1}^{b} k_i'$, and $K_{s4} = \sum_{i=b}^{n+1} k_i'$; $K_{b1} = EA/L_a$, $L_a = (a\text{-}1)L + 0.5L$, $K_{b2} = EA/L_b$, and $L_b = (b\text{-}a)L$. K_{b1} and K_{b2} represent the axial linear stiffness of the deformed beam, EA represents the tensile and compressive stiffness of the beam, L_a and L_b denote the total length of the beam considering axial deformation, L denotes the single-span span, k_i' represents the lateral stiffness of the i-th general story column, and k_{br} represents the lateral stiffness of the brace.

2.4 Influence of multi-span brace arrangement locations on the lateral resistance performance of structural floors

Expanding the brace arrangement principle to n-span configurations was conducted to assess the influence of lateral stiffness on the structural layer. By dividing the structure at the brace node, there was a substructure comprising frame columns preceding the brace node. The stiffness between brace nodes was evenly distributed on both sides, with the brace and frame after the brace node treated as separate substructures. It was essential to account for the axial deformation in the frame beams before, between, and after the braces. The overall structural stiffness was subsequently determined by iterative calculations of the equivalent substructure stiffness.

The formula is expressed as follows:

Fig. 13 Random arrangement of n-span general steel frame brace a and b spans
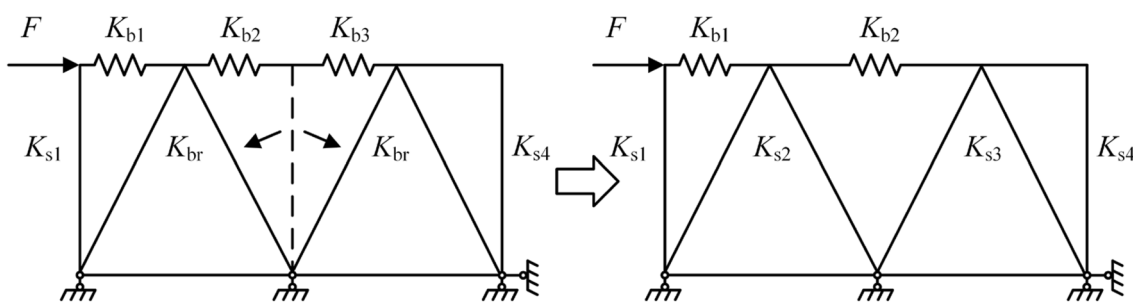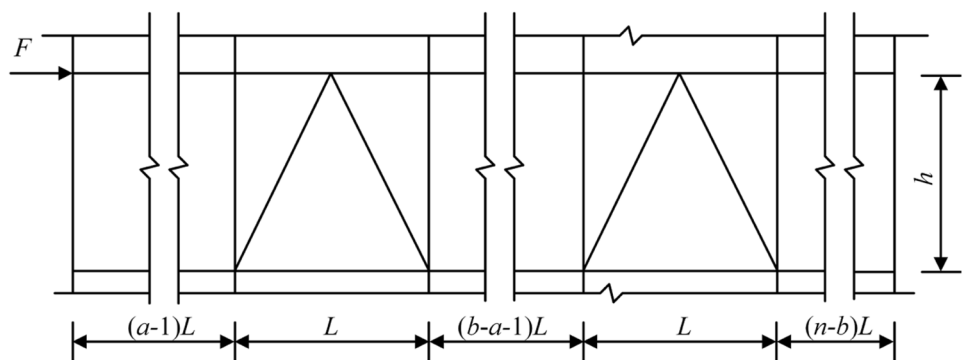
Fig. 14 Calculation diagram of random arrangement of brace double-span general layer

$$\begin{cases} K_{1...n} = K_1 + \dfrac{1}{1/K_{2...n} + 1/K_{b1}} \\ K_{i...n} = K_i + \dfrac{1}{1/K_{i+1...n} + 1/K_{bi}} \end{cases}, \tag{14}$$

where $K_{1...n}$ represents the structural layer stiffness of n substructures, $K_{i...n}$ represents the overall structural layer stiffness of substructures i–n, and K_{bi} represents the axial stiffness of the beam in part i.

2.5 Finite element modeling and validation

Finite element analysis was conducted using the ABAQUS software to create a model of the center brace steel frame, as depicted in Fig. 15. The model employed a Q345 steel material, and the primary model selected was the triple-folding line model. Welded connections were implemented between the braces, nodal plates, beams, and columns in the finite element model of the center brace steel frame. These connections were simplified and treated as rigid. ABAQUS software utilizes a TIE contact relationship to simulate the interaction between the connected components (Ghannadi et al. 2023). Finite element models of the center brace steel frames were constructed using C3D8R cells (Imran et al. 2023). Meshing was performed at intervals of 50 mm longitudinally and 15 mm across the cross section, with three meshes in the thickness direction for each component (Ling et al. 2022). The mesh convergence was validated, indicating that the mesh sensitivity did not notably increase with the additional meshes. Therefore, the aforementioned

mesh-partitioning approach was suitable. To improve the convergence of the finite element model and mitigate the stress concentration resulting from the load application at a single point during the analysis, the top column loading surface was coupled to a point using the coupling command (Tran-Ngoc et al.2022). Subsequently, a monotonic displacement load was applied, which was set to 1/50 of the story height. This approach facilitates an even load distribution and improves the convergence of the analysis.

Utilizing the modeling approach outlined earlier, we constructed a corresponding finite element model based on the static pushover test data from a one-bay, single-span, three-story herringbone brace frame, as conducted by Existing experiments (Yang et al. 2010) as presented in Fig. 16. The geometric structure of the specimen is designed as follows. The column had a cross section of HW150×150×7×10, the top beam had a cross section of HW200×150×6×9, the first- and second-floor beams had cross sections of HW150×100×6×9, and the brace had a cross section of HN100×50×5×7. The structural steel used was Q235B, with a yield strength of 235 MPa.

A gradual displacement load of 100 mm was systematically applied at the point, where lateral coupling of the top column was located. This procedure yielded load–displacement curves (Fig. 17d) and facilitated the observation of deformation patterns in the specimens (Fig. 17a–c). Notably, when subjected to the peak load, the first- and second-floor braces exhibited out-of-plane buckling behavior, whereas the third-floor braces displayed similar out-of-plane buckling at a load displacement of 35 mm. These deformation patterns closely mirrored the test results. Importantly, the
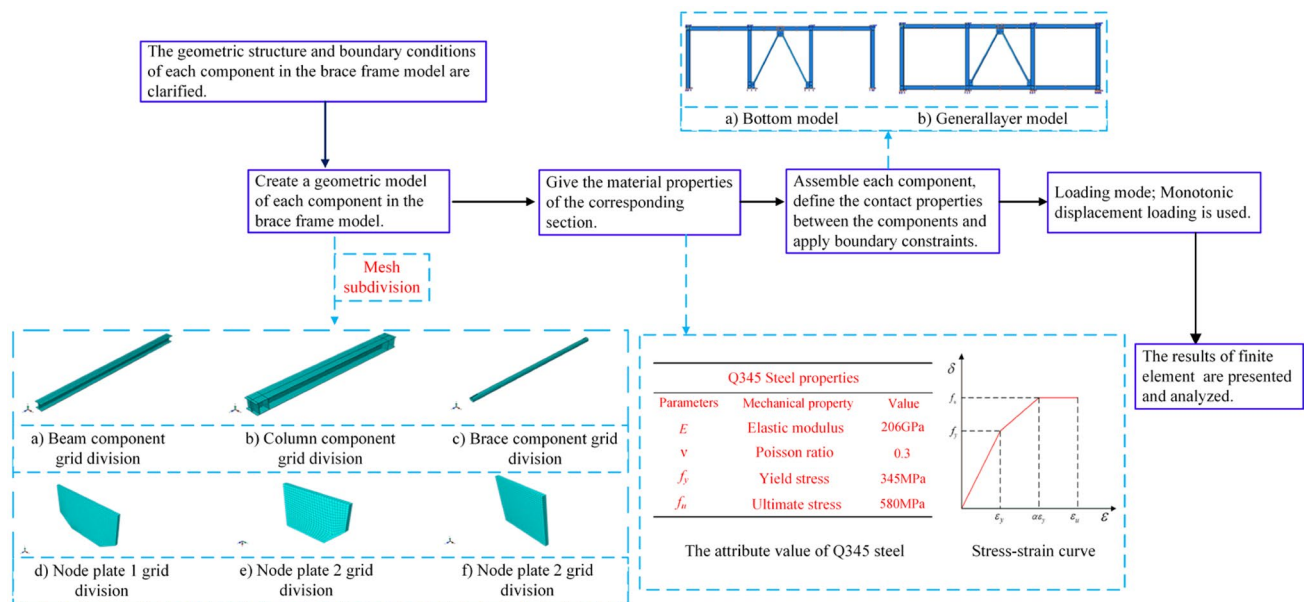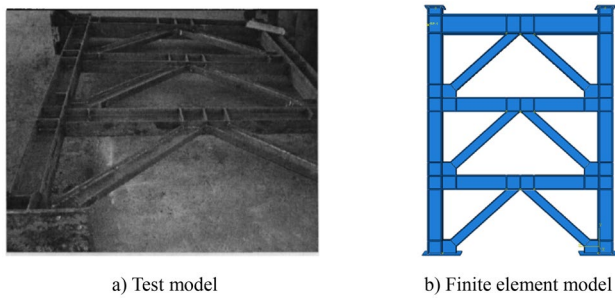

Fig. 15 Modeling process of center brace steel frame

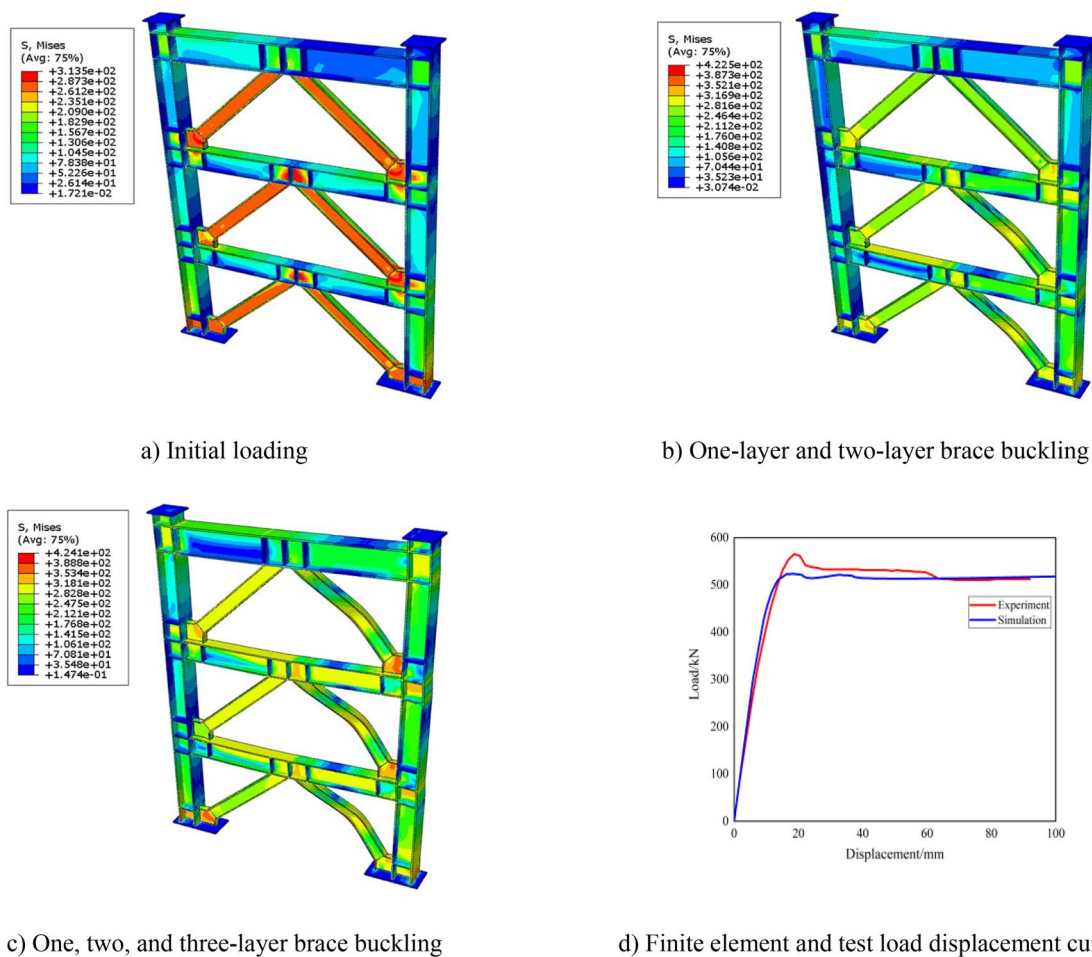a) Test model   b) Finite element model

Fig. 16 Test and finite element model diagram. **a** Test model, **b** Finite element model

load–displacement curves obtained through the finite element simulation exhibited a precise fit with the test curves, thus establishing the robustness of the finite element model.

Utilizing the previously outlined modeling approach, we established a finite element model for the center brace steel frame. The frame layer, characterized by a 6000 mm span and 4000 mm height, is subjected to various span configurations, including three spans, five spans, and seven spans, both for the bottom floor and general floor finite element analysis models. These models are systematically denoted following the convention SC-(number of spans in the layer)-(position of the brace arrangement within the spans). Additionally, diverse brace arrangements, such as single-, double-, and three-span arrangements at various positions, have been considered, leading to a comprehensive set of 190 distinct finite element models.

The beam cross section measured $HW250 \times 250 \times 9 \times 14$, whereas the column cross section was $HW344 \times 354 \times 16 \times 16$. The brace consisted of a round steel pipe with dimensions $\Phi140 \times 13$. All the structural components were constructed from Q345 steel. Schematic diagrams depicting the various span arrangements of the braces are shown in Fig. 18.

a) Initial loading

b) One-layer and two-layer brace buckling

c) One, two, and three-layer brace buckling

d) Finite element and test load displacement curves

Fig. 17 Specimen deformation law, finite element, and test load–displacement curves. **a** Initial loading, **b** One-layer and two-layer brace buckling, **c** One, two, and three-layer brace buckling, **d** Finite element and test load–displacement curves

Where SC-bottom layer/standard layer-span number-brace arrangement span position, D represents the bottom layer, and T represents the standard layer.

Table 1 summarizes the finite element models developed to examine the various positional arrangements of the three-, five-, and seven-span bottoms and general floor braces. Through the creation and analysis of a comprehensive set of 190 finite element models encompassing both the bottom and general floors, we computed the lateral stiffness values for these structural layers.

Concurrently, the theoretical stiffness values for various brace span arrangements within the structural layer were computed. Additionally, an error analysis was conducted to compare the theoretical calculations with the results obtained through the finite element analysis. As depicted in Fig. 19, the maximum error between the theoretical calculations and the finite element analysis results was approximately 15%. The theoretical analytical model exhibited commendable accuracy, with the calculation results displaying a high degree of consistency. Importantly, the theoretical results derived from the method proposed in this study tend to be more conservative than their finite element counterparts, offering a substantial safety margin.
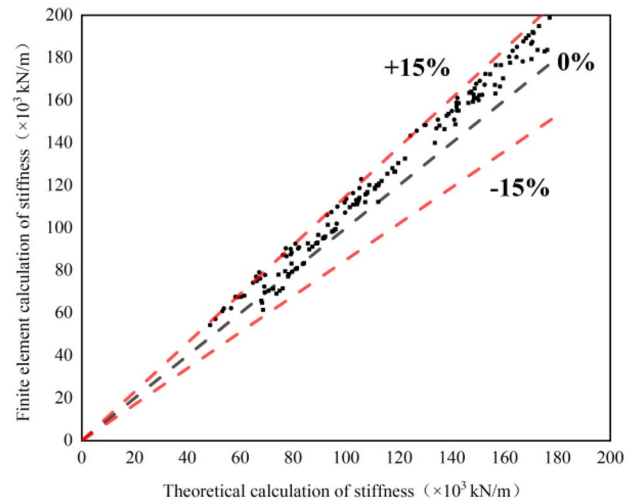

Fig. 19 Comparative analysis of theoretical model calculation stiffness and finite element calculation stiffness

2.6 The impact on the lateral resistance of frame brace structural systems

In this section, the influence of the stiffness of each member in the frame brace system on the overall lateral stiffness of

Fig. 18 The various span arrangements of the braces. **a** SC-D-5-25, **b** SC-T-5-145, **c** SC-D-7-126, **d** SC-T-7-23
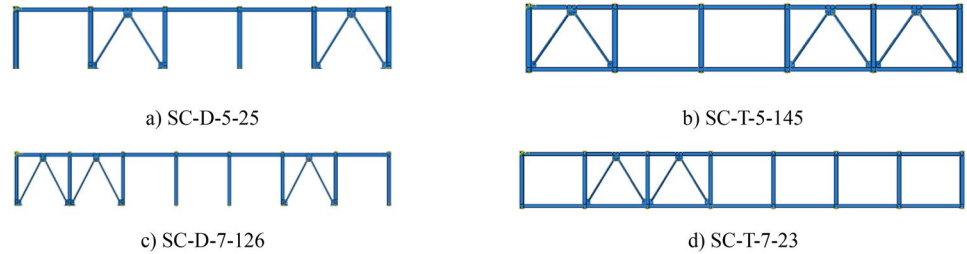

a) SC-D-5-25

b) SC-T-5-145

c) SC-D-7-126

d) SC-T-7-23

Table 1 Finite element model number

Frame layer finite element model number (D/T)						
SC-3-1	SC-3-2	SC-3-3	SC-3-12	SC-3-13	SC-3-23	SC-3-123
SC-5-1	SC-5-2	SC-5-3	SC-5-4	SC-5-5	SC-5-12	SC-5-13
SC-5-14	SC-5-15	SC-5-23	SC-5-24	SC-5-25	SC-5-34	SC-5-35
SC-5-45	SC-5-123	SC-5-124	SC-5-125	SC-5-134	SC-5-135	SC-5-145
SC-5-234	SC-5-235	SC-5-245	SC-5-345	SC-7-1	SC-7-2	SC-7-3
SC-7-4	SC-7-5	SC-7-6	SC-7-7	SC-7-12	SC-7-13	SC-7-14
SC-7-15	SC-7-16	SC-7-17	SC-7-23	SC-7-24	SC-7-25	SC-7-26
SC-7-27	SC-7-34	SC-7-35	SC-7-36	SC-7-37	SC-7-45	SC-7-46
SC-7-47	SC-7-56	SC-7-57	SC-7-67	SC-7-123	SC-7-124	SC-7-125
SC-7-126	SC-7-127	SC-7-134	SC-7-135	SC-7-136	SC-7-137	SC-7-145
SC-7-146	SC-7-147	SC-7-156	SC-7-157	SC-7-167	SC-7-234	SC-7-235
SC-7-236	SC-7-237	SC-7-245	SC-7-246	SC-7-247	SC-7-256	SC-7-257
SC-7-267	SC-7-345	SC-7-346	SC-7-347	SC-7-356	SC-7-357	SC-7-367
SC-7-456	SC-7-457	SC-7-467	SC-7-567			

the structure was analyzed. This analysis helps clarify the main mechanical parameters that affect the lateral stiffness of the frame brace structure and explore the factors that influence the structural stiffness.

By the principle of virtual work

$$\Delta = \sum \int \frac{M_1 M_P}{EI} ds + \sum \int \frac{N_1 N_P}{EA} ds + \sum \int \frac{k Q_1 Q_P}{GA} ds, \tag{15}$$

where N_1, M_1, and Q_1 denote the internal forces of the member under a unit load; N_P, M_P, and Q_P denote the internal forces of the member caused by the actual load; EI, EA, and GA represent the bending, axial, and shear stiffnesses of the member, respectively; and k denotes the shear strain cross-sectional shape factor.

Equation (15) demonstrates that the lateral displacement of the structure is not solely determined by the internal forces acting on the members but is also influenced by the stiffness characteristics of each member. Upon a more comprehensive examination of the overall structural lateral stiffness, it is evident that this collective stiffness comprises various stiffness components. Furthermore, these individual member stiffnesses exerted varying degrees of impact on the overall structural lateral stiffness. To delve further into this, we analyzed the effects of bending and axial stiffness exhibited by different members on the overall lateral stiffness of

the structure. A single structural module featuring a herringbone brace and an X-type arrangement was constructed by applying an identical lateral concentrated load of 100 kN to the top floor, as shown in Fig. 20a. Furthermore, Fig. 20b presents the overall structure composed of four structural modules. The effects of the axial, bending, and shear stiffness of each member on the maximum lateral displacement of the top floor were examined, considering varying numbers of modules ($N=1, 2, 3, 4, 5$).

The single-module structure boasts a span of 24 m and floor height of 16 m, as depicted in Fig. 20a. The key structural elements include HW250×250×9×14 for the beam cross section, HW344×354×16×16 for the column cross section, and Φ70×6 round steel pipe for the brace. All components were constructed using Q345 steel, and it is pertinent to note that rigid connections were employed for the structural nodes.

The results presented in Fig. 21 show the prominent role of the brace axial stiffness in shaping the maximum lateral displacement of the structure. These braces are instrumental in endowing the structure with shear lateral stiffness primarily through axial deformation. As the height of the structure increased, the axial stiffness of the columns became more significant in bolstering the overall stiffness. Furthermore, the frame columns substantially contribute to the bending lateral stiffness of the structure, mainly through axial
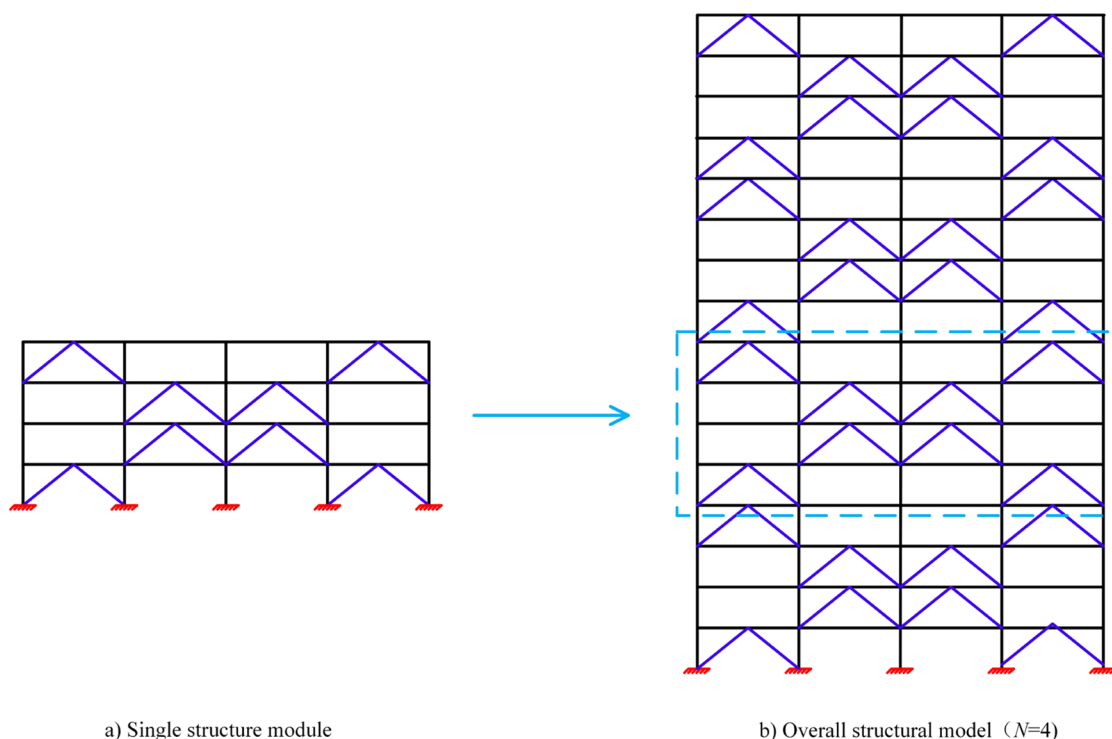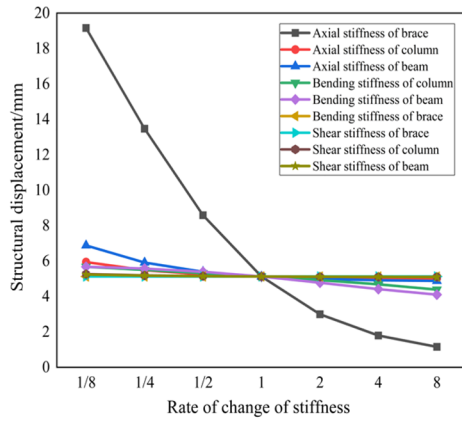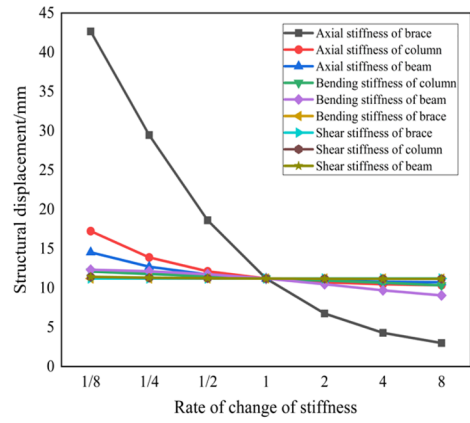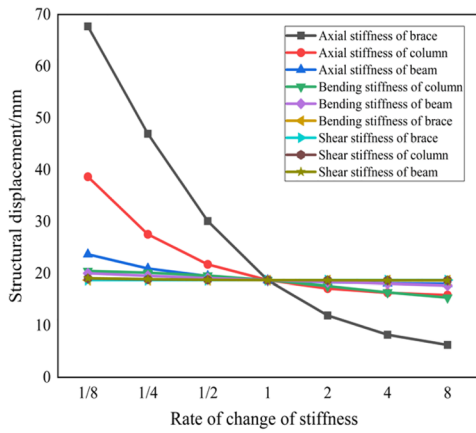

a) Single structure module

b) Overall structural model（N=4)

Fig. 20 Structural model

a) Influence of component stiffness on the lateral displacement of the structure (*N*=1)

b) Influence of component stiffness on the lateral displacement of the structure (*N*=2)

c) influence of component stiffness on the lateral displacement of the structure (*N*=3)

d) Influence of component stiffness on the lateral displacement of the structure (*N*=4)

e) Influence of component stiffness on the lateral displacement of the structure (*N*=5)

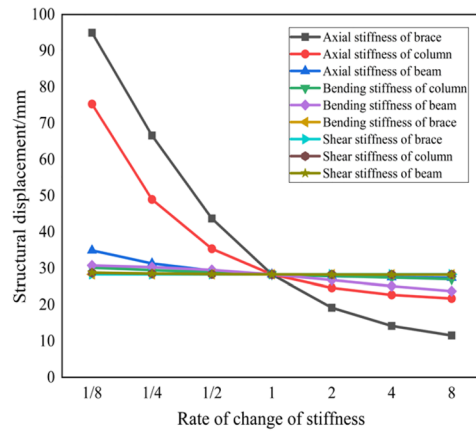◄**Fig. 21** Influence of component stiffness on the lateral displacement of the overall structure. **a** Influence of component stiffness on the lateral displacement of the structure ($N=1$), **b** Influence of component stiffness on the lateral displacement of the structure ($N=2$), **c** influence of component stiffness on the lateral displaceme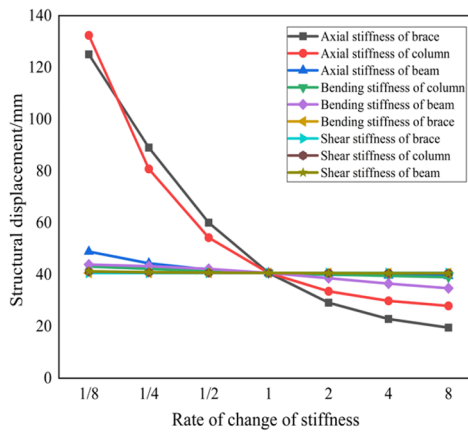nt of the structure ($N=3$), **d** Influence of component stiffness on the lateral displacement of the structure ($N=4$), **e** Influence of component stiffness on the lateral displacement of the structure ($N=5$)

deformation. Conversely, the bending and shear stiffnesses of the structural members exerted a minimal influence on the overall lateral stiffness of the structure. Notably, the brace and column axial stiffnesses dominate in determining the lateral stiffness of the structure, impacting both the shear and bending lateral stiffness through their respective axial deformations.

In a frame bracing system, the predominant lateral stiffness of the structure is attributed to the axial stiffness of braces and columns. This emphasizes the importance of the axial stiffness of the components within a frame-braced structural system. Assuming a negligible influence of bending moments and shear forces on structural displacement and only considering the impact of axial forces in the components, the frame bracing system can be simplified for truss structure analysis. Consequently, the displacement and stiffness of the structure under a horizontal load P were calculated using Eq. (16).

$$\begin{cases} \Delta = \sum \int \dfrac{N_1 N_P}{EA} ds = \sum_{i=1}^{n} \dfrac{P N_1^2 l_i}{EA_i} \\ K = \dfrac{P}{\Delta} = 1 / \sum_{i=1}^{n} \dfrac{N_i^2 l_i}{EA_i} = 1 / \sum_{i=1}^{n} \dfrac{N_i^2}{i_i} \end{cases}, \tag{16}$$

where $i_i = EA_i/l_i$ is the axial stiffness of the i-th member, N_i is the axial force of the i-th component under a unit load, and n is the total number of components.

3 Positional parameter optimization for center brace arrangement

Further analysis was conducted to investigate the load transfer mechanisms associated with various brace arrangement positions and identify the optimal brace arrangement. The objective of this study was to develop a methodology for determining the optimal brace arrangement.

3.1 Optimization arrangement analysis of the center brace

In this study, the brace layout was optimized by maximizing the lateral stiffness of the structure. In the simplified Eq. (16) for stiffness, enhancing the lateral stiffness of the structure

can be achieved by reducing $\sum_{i=1}^{n} \frac{N_i^2}{i_i}$, implying that the lateral stiffness increases when the braces are arranged such that $|N_i| \to 0$. The goal was to tackle the challenge of brace arrangement by strategically positioning the braces to minimize the presence of zero-force members, while maintaining a uniform and minimal distribution of internal forces among the other members. The optimization process adheres to fundamental structural principles (Tianjian 2003), emphasizing direct internal force transfer, even distribution of internal forces across all members, and minimization of the internal forces within each member.

Hence, the aim of our investigation is to identify the optimal brace arrangement that facilitates the most straightforward force transfer. Chen et al. established the utility of the bearing factor, denoted as G, which serves as a quantitative measure for assessing the extent of direct force transfer within a structural system (Chen and Jin 2011). This quantification is mathematically expressed by Eq. (17).

$$\min G = \sum_{i=1}^{n} |N_i l_i|, \tag{17}$$

where G represents the load factor, N_i represents the axial force of the i-th member under a unit load, l_i represents the member length, and n denotes the total number of members.

3.2 Optimization arrangement principle of the center brace

The investigation also delved into how the vertical placement of the brace arrangement between floors influences the distribution of internal forces among structural members. The analysis began with an evaluation of a fundamental brace unit consisting of braces, beams, and columns. When a unit force of 1 was applied to the basic brace unit, horizontal loads were transmitted along the members to the floor below. This resulted in the augmentation of both the internal forces within the member and vertical load transferred to the lower main structure. Consequently, a combination of tension and compression forces emerged, as shown in Fig. 22.

Note: Positive by tension and negative by pressure.

(1) When arranging the upper-side span braces, there are three possible positions for the lower braces: directly below the upper braces, diagonally below the upper braces, or diagonally below another span, as shown in Fig. 23. The axial force diagrams for these three lower brace arrangements when subjected to a unit force of 1 applied to the top layer are presented in Fig. 23.

Several observations can be made from Fig. 23. In cases (a) and (b), the impacts of the brace and column on the structural load factor were identical. In (a), the
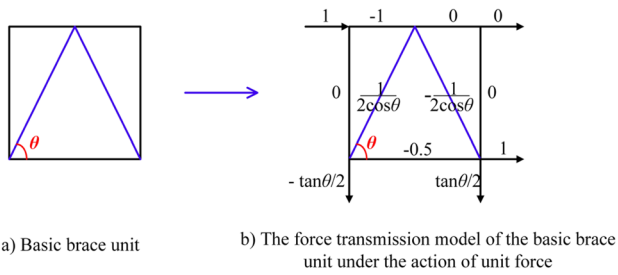
a) Basic brace unit

b) The force transmission model of the basic brace unit under the action of unit force

Fig. 22 Basic brace and force transmission model under unit force

vertical force generated by the two basic brace units was further amplified through superposition and transferred to the lower main structure. Conversely, in (b), the vertical force produced by the two basic brace units was effectively canceled out through a combination of tension and compression forces, resulting in a net force of 0. Consequently, when compared to (a), the vertical load transmitted from the structure to the lower part of the main structure in (b) was halved. This reduction minimized the vertical force on the lower part of the structure, optimized the structural stress, decreased the structural load factor, and enhanced the force transmission efficiency along the structural path. In contrast, (c) can be seen as an extension of (b), where the two basic brace units were connected by

a beam. However, it was evident that the basic brace units remained independent, and the vertical forces generated by these units did not cancel out. Instead, they increased the internal forces within the beam. Consequently, the intended improvement in the force transfer path was not effectively achieved. Therefore, the arrangement of the diagonal underside of the brace span was not discussed further in subsequent sections of this study.

During the assembly of basic units, the magnitude of the horizontal load remained constant. Consequently, it is advantageous to minimize the horizontal load transfer path and prevent the accumulation of vertical loads within the basic brace unit. To achieve this objective, the ideal positional relationship between the lower layer of the brace and the current layer of the brace is to position the lower layer diagonally beneath the current layer of the brace in the pro-span. This arrangement optimizes the load transfer and minimizes vertical load accumulation within the structure. Thus, positioning the lower braces diagonally beneath the pro-span is preferable when arranging the upper braces for side span brace configurations. This arrangement can be represented numerically in the following matrix format:

$$\begin{matrix} \Lambda & 0 \\ 0 & 0 \end{matrix} \rightarrow \begin{matrix} \Lambda & 0 \\ 0 & \Lambda \end{matrix} \quad \text{or} \quad \begin{matrix} 0 & \Lambda \\ 0 & 0 \end{matrix} \rightarrow \begin{matrix} 0 & \Lambda \\ \Lambda & 0 \end{matrix}$$

a) Arrangement under the brace and axial force diagram

b) Arrangement under the brace and axial force diagram

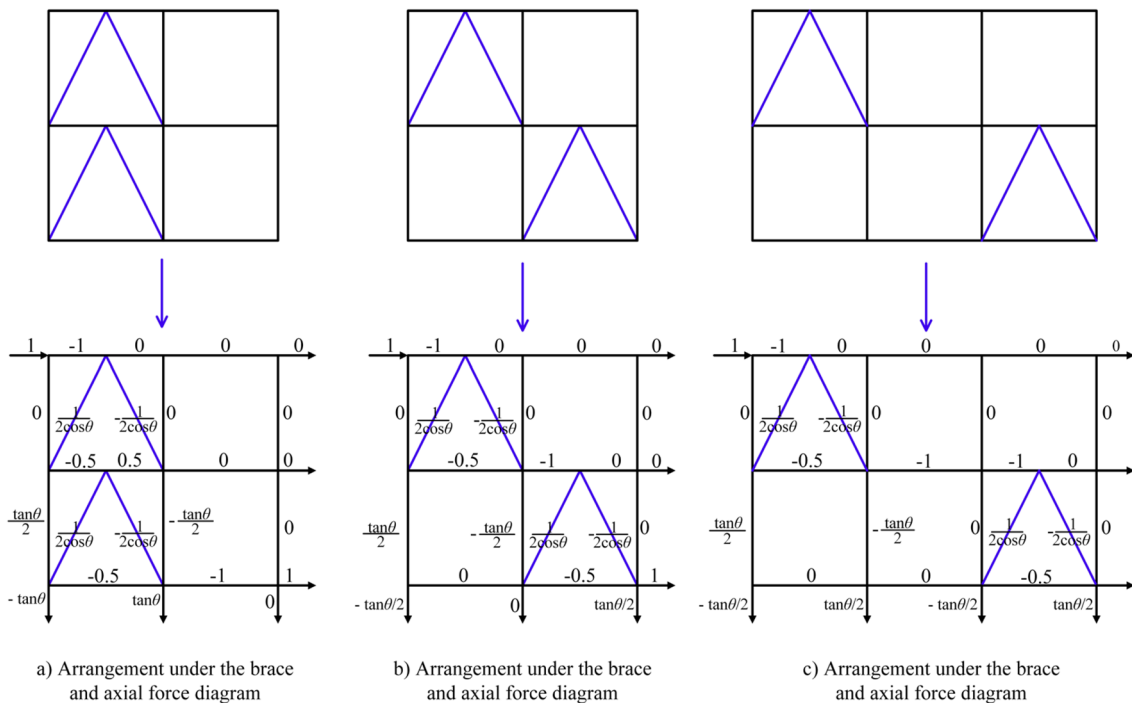c) Arrangement under the brace and axial force diagram

Fig. 23 Lower brace arrangement and axial force diagram

Note: "Λ" denotes the current brace arrangement position, "Λ" signifies the preferred brace arrangement location, and "0" indicates the absence of a brace arrangement. The same notation was applied in the following subsections.

(2) When arranging the upper intermediate braces in a single-span configuration, there are two possible lower brace arrangements to consider, as depicted in Fig. 24. Lower braces can be positioned directly below the upper brace or diagonally below either the left or the right side of the upper brace. Figure 23 illustrates the axial force diagram for the lower brace arrangement when subjected to a unit force of 1 applied at the top level.

In Fig. 24, the brace and columns within the entire direct-influence area exhibit identical bearing factors in the structure. When the upper-layer brace was positioned at a specific location, the magnitude of the axial force exerted by the lower-layer columns remained constant. Notably, the bearing factor in (a) was smaller than those in (b) and (c), indicating that the load transferred to the lower main structure was reduced by half in (a) and (b) compared to (c). This significant reduction in the load on the lower main structure demonstrated the effectiveness of the brace arrangement in minimizing the structural

load. Considering the load symmetry, this study suggests that when arranging a brace for a single span at any intermediate position on the top floor, the lower brace should be positioned diagonally below the particular brace. This arrangement is represented by the following numerical matrix:

$$
\begin{matrix} 0 & \Lambda & 0 \\ 0 & 0 & 0 \end{matrix} \rightarrow
\begin{matrix} 0 & \Lambda & 0 \\ \Lambda & 0 & 0 \end{matrix} \text{ or }
\begin{matrix} 0 & \Lambda & 0 \\ 0 & 0 & \Lambda \end{matrix}
$$

(3) The brace arrangement for multiple spans can be conceptualized as a hybrid of single- and double-span arrangements. For illustration purposes, we considered a double-span brace arrangement.

The double-span brace arrangement entails separation of the braces and can be represented by the following matrix:

$$
\begin{matrix} 0 & \Lambda & 0 & \Lambda & 0 \\ 0 & 0 & 0 & 0 & 0 \end{matrix} \rightarrow
\begin{matrix} 0 & \Lambda & 0 & 0 & 0 \\ \Lambda & 0 & \Lambda & 0 & 0 \end{matrix} +
\begin{matrix} 0 & 0 & 0 & \Lambda & 0 \\ 0 & 0 & \Lambda & 0 & \Lambda \end{matrix} \rightarrow
\begin{matrix} 0 & \Lambda & 0 & \Lambda & 0 \\ \Lambda & 0 & \Lambda & 0 & \Lambda \end{matrix}
$$

a) Arrangement under the brace and axial force diagram

b) Arrangement under the brace and axial force diagram

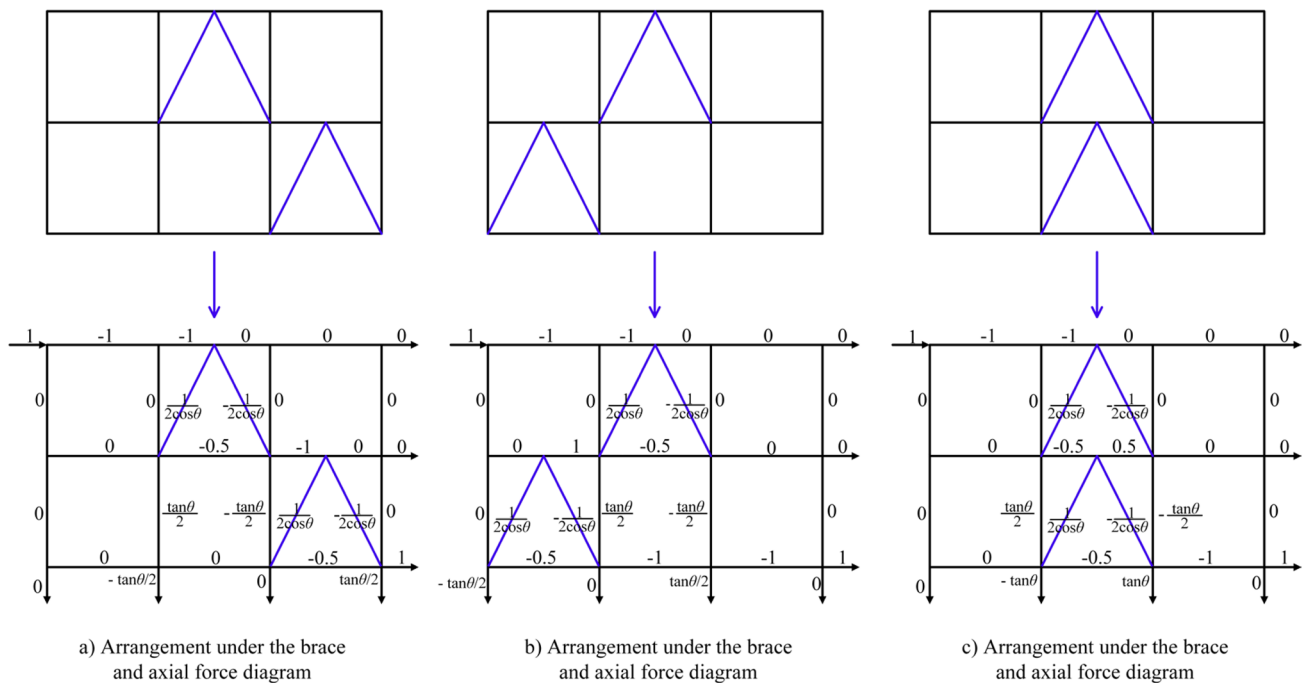c) Arrangement under the brace and axial force diagram

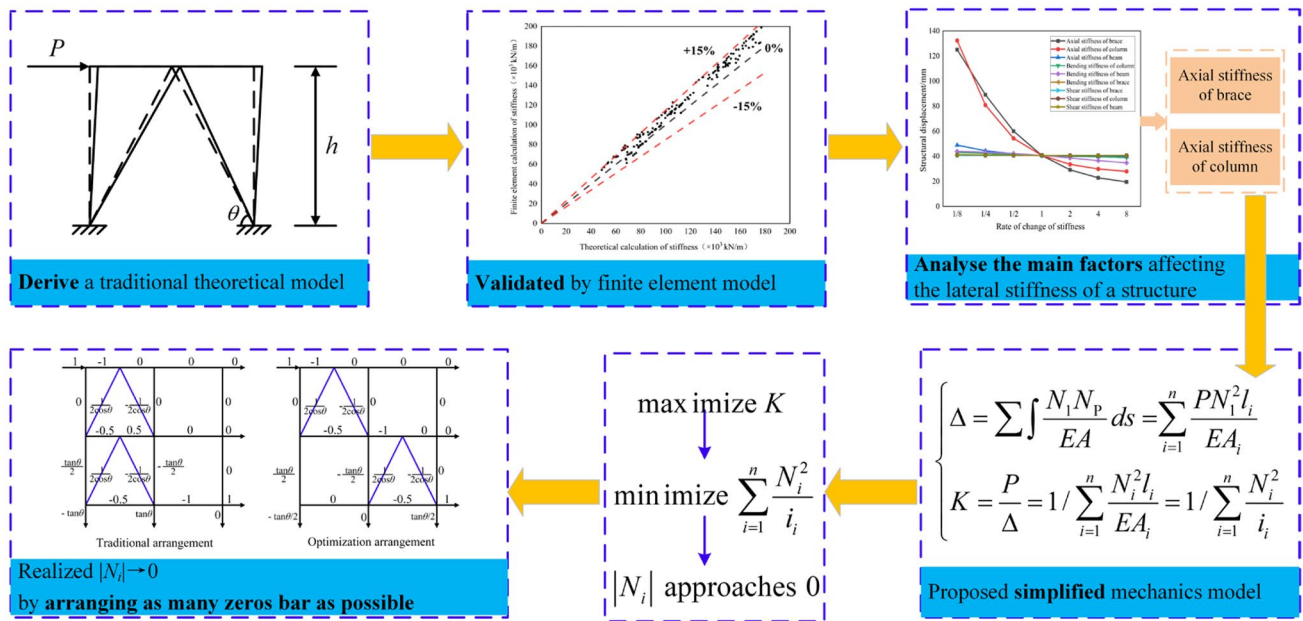**Fig. 24** Lower brace arrangement and axial force diagram

Fig. 25 Optimization method for the arrangement of center brace

The continuous arrangement of the double-span brace in the center can be represented by the following matrix:

$$
\begin{matrix}
0 & \Lambda & \Lambda & 0 \\
0 & 0 & 0 & 0
\end{matrix}
\rightarrow
\begin{matrix}
0 & \Lambda & 0 & 0 \\
\Lambda & 0 & \Lambda & 0
\end{matrix}
+
\begin{matrix}
0 & 0 & \Lambda & 0 \\
0 & \Lambda & 0 & \Lambda
\end{matrix}
\rightarrow
\begin{matrix}
0 & \Lambda & \Lambda & 0 \\
\Lambda & 0 & 0 & \Lambda
\end{matrix}
$$

The continuous arrangement of the double-span brace at the side spans can be represented by the following matrix.

$$
\begin{matrix}
\Lambda & \Lambda & 0 & 0 \\
0 & 0 & 0 & 0
\end{matrix}
\rightarrow
\begin{matrix}
\Lambda & 0 & 0 & 0 \\
0 & \Lambda & 0 & 0
\end{matrix}
+
\begin{matrix}
0 & \Lambda & 0 & 0 \\
0 & 0 & \Lambda & 0
\end{matrix}
\rightarrow
\begin{matrix}
\Lambda & \Lambda & 0 & 0 \\
0 & \Lambda & \Lambda & 0
\end{matrix}
$$

The continuous arrangement of the brace multi-span (considering symmetry) can be represented using the following matrix:

$$
\begin{matrix}
0 & \Lambda & \Lambda & \Lambda & 0 & 0 \\
0 & 0 & 0 & 0 & 0 & 0
\end{matrix}
\rightarrow
\begin{matrix}
0 & \Lambda & 0 & 0 & 0 & 0 \\
\Lambda & 0 & 0 & 0 & 0 & 0
\end{matrix}
+
\begin{matrix}
0 & \Lambda & 0 & 0 & 0 & 0 \\
0 & 0 & \Lambda & 0 & 0 & 0
\end{matrix}
+
\begin{matrix}
0 & \Lambda & 0 & 0 & \Lambda & 0 \\
0 & 0 & 0 & \Lambda & 0 & \Lambda
\end{matrix}
\rightarrow
\begin{matrix}
0 & \Lambda & \Lambda & \Lambda & 0 \\
\Lambda & 0 & \Lambda & 0 & \Lambda
\end{matrix}
$$

(4) Brace optimization arrangement method.

Based on the preceding analysis, it is evident that placing the lower layer of braces diagonally below the upper layer is a suitable strategy. This arrangement effectively mitigates vertical force transmission from the basic brace unit to the lower structural components. Conversely, when positioning the lower layer of braces, it is advisable to place them directly beneath the upper layer of braces. In this case, the lower portion served as the foundation and increasing the vertical force transmitted to it did not significantly affect the overall structure. The primary objective is to minimize the horizontal load transferred to the beam. Therefore, it is recommended to arrange braces in the upper layer directly below the lower layers. Simultaneously, it was essential to avoid excessive disparities in the number of braces within each span. A significant number

of braces within the same span led to a substantial vertical force superposition generated by the basic brace units. Conversely, an offset brace in the span-wise direction results in reduced vertical forces, which are less effective in decreasing the transmission of vertical forces to the lower portion of the main structure. Figure 25 illustrates the entire process of the steel frame center brace optimization arrangement method proposed in this study.

4 Static lateral performance of steel frame with optimized center brace arrangement

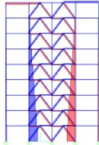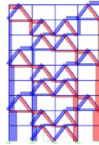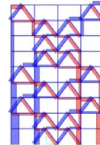## 4.1 The effect of the optimized center brace arrangement on the structural lateral performance
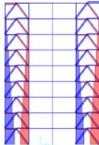
This study illustrates a nine-story steel frame structure with four spans. Each story was maintained at a height of 4 m and the column-to-column span was 6 m. The structural brace featured two spans per story. A central force of 100 kN was applied to the top of the structure, symmetrically divided into 50 kN loads for both the left and right sides to account for the structural symmetry.
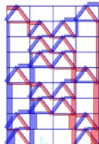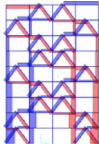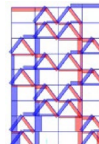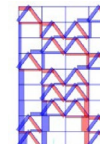
The structural configuration included variable cross sections for both beams and columns for every three stories. For the first through third stories, $HW400 \times 400 \times 15 \times 15$ columns and $HN400 \times 200 \times 8 \times 13$ beams were used. On the fourth to sixth stories, $HW350 \times 350 \times 10 \times 16$ columns and $HN400 \times 200 \times 7 \times 11$ beams were used, respectively. Finally, for the seventh to ninth stories, $HW300 \times 300 \times 15 \times 15$ columns and $HN400 \times 150 \times 8 \times 13$ beams, respectively, were employed. The brace components consisted of round steel pipes with a diameter of $\Phi140 \times 9$. All the structural members were constructed using Q345 steel. Structural modellng and analysis were conducted using SAP2000 software.

This study primarily investigated the influence of brace arrangement position on structural lateral performance. This involved a comparative analysis between the traditional brace arrangement (centralized and two-sided) and an optimized brace arrangement. The results of this analysis are summarized in Tables 2 and 3, which provide a comprehensive overview of the structural lateral performance under both arrangements.

Table 2 Comparison of lateral resistance of structures with different brace arrangements

Position of the brace arrangement	Traditional arrangement 1	Traditional arrangement 2	Optimized arrangement 1	Optimized arrangement 2
Axial force diagram of brace arrangement				
Maximum lateral displacement of the top floor (mm)	12.01	8.11	5.80	5.81
Lateral stiffness (kN/m)	8.33×10^3	12.33×10^3	17.23×10^3	17.22×10^3
Maximum axial force of bottom column (kN)	229.79	205.77	102.53	104.20

Table 3 Comparison of lateral resistance of structures with different brace arrangements

Position of the brace arrangement	Optimized arrangement 3	Optimized arrangement 4	Optimized arrangement 5	Optimized arrangement 6
Axial force diagram of brace arrangement				
Maximum lateral displacement of the top floor (mm)	5.78	5.99	6.06	5.77
Lateral stiffness (kN/m)	17.30×10^3	16.67×10^3	16.51×10^3	17.32×10^3
Maximum axial force of bottom column (kN)	105.48	106.78	107.58	104.01

The results in Tables 2 and 3 demonstrate the following observations:

(1) The positioning of the brace arrangement had a notable impact on both the maximum lateral displacement of the top floor and lateral stiffness of the structure when all other conditions remained the same. The optimized brace arrangement notably enhanced the lateral performance of the structure and effectively boosted the lateral capacity of its components.

(2) Compared to the traditional brace arrangement, the structures with optimized brace arrangements exhibited significantly higher resistance to the lateral displacement. The reduction ranged from 52% to a noteworthy extent, with the maximum lateral displacement decreasing from 12.01 mm to a range of 5.77–6.06 mm.

(3) Between the traditional centralized brace arrangement and two-sided brace arrangement, the former proved superior. The centralized brace arrangement, positioned on the center column, generated both tension and compression axial forces, resulting in decreased internal forces within the structural members and an augmented lateral stiffness for the structure.

(4) The optimized brace arrangement contributed to a more uniform distribution of internal forces within the structural members, which in turn enhanced the lateral stiffness. In contrast, a traditional brace arrangement often leads to substantial axial forces on bottom column members. Notably, in the optimized brace arrangement, the maximum axial force experienced by the bottom column was more than 50% lower than that in the traditional brace arrangement.

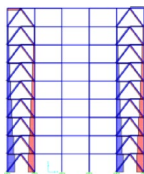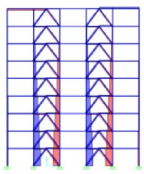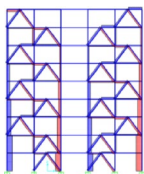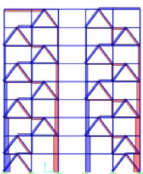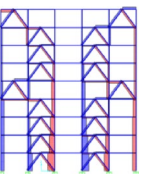In practical scenarios with consistent hole locations in the vertical direction, such as elevator doorways, the conclusions drawn from previous brace arrangement analyses may not be applicable. Therefore, it is imperative to incorporate constraints on brace arrangement location. In this study, we assessed the optimal brace arrangement within the context of a one-bay, five-span, nine-story frame utilizing an elevator doorway as an exemplar constraint. The chosen cross sections remained consistent with the four-span model. A detailed description of these schemes is provided in Table 4.
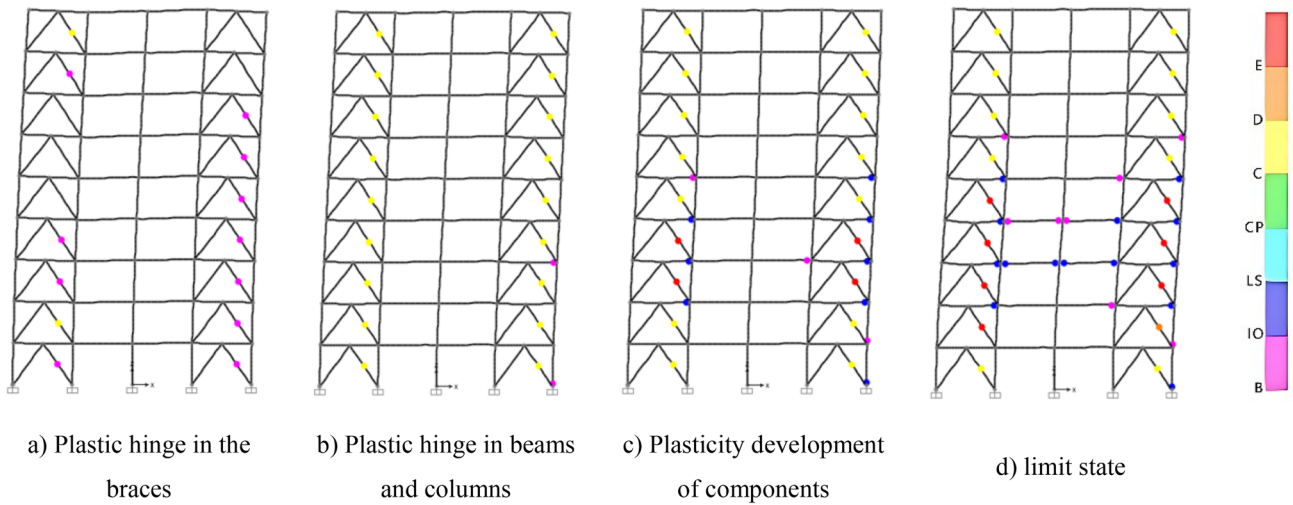
The results presented in Table 4 reveal that the maximum lateral displacement of the top floor of the structure was approximately 40% smaller when the brace was optimally arranged compared with the traditional brace configuration. However, when comparing the four-span and nine-floor models, it became apparent that the effect of optimizing the brace arrangement was somewhat attenuated because of the absence of a brace in the central span, rendering the left and right sides of the structure as functionally independent. Nevertheless, a notable improvement in lateral resistance persists, underscoring the efficacy of the brace arrangement optimization method. Furthermore, it is evident that by adhering to the brace arrangement rules, the structural force transmission pathway can be enhanced, promoting uniform and minimized internal forces within the structural members and bolstering the structure's lateral performance. By contrast, traditional brace arrangements often lead to substantial axial forces borne by the bottom column members, further confirming that adhering to brace arrangement guidelines can swiftly yield well-structured brace arrangements with heightened stiffness.

4.2 Pushover analysis of steel frame with optimized center brace arrangement

After optimizing the arrangement of braces in the structural scheme, a static pushover analysis was conducted. The goal

Table 4 Comparison of the lateral resistance of structures with different brace arrangements considering building functions

Position of the brace arrangement	Traditional arrangement 1	Traditional arrangement 2	Optimized arrangement 1	Optimized arrangement 2	Optimized arrangement 3
Axial force diagram of brace arrangement					
Maximum lateral displacement of the top floor (mm)	11.46	10.27	6.94	7.04	7.16
Lateral stiffness (kN/m)	8.73×10^3	9.74×10^3	14.40×10^3	14.20×10^3	13.98×10^3
Maximum axial force of bottom column (kN)	219.63	167.38	122.88	129.53	140.33

a) Plastic hinge in the braces

b) Plastic hinge in beams and columns

c) Plasticity development of components

d) limit state

Fig. 26 Sequence and location of plastic hinge formation in braces of the traditional arrangement structure. **a** Plastic hinge in the braces, **b** Plastic hinge in beams and columns, **c** Plasticity development of components, **d** limit state

a) Plastic hinge in the braces

b) Plastic hinge in beam end

c) Plasticity development of components
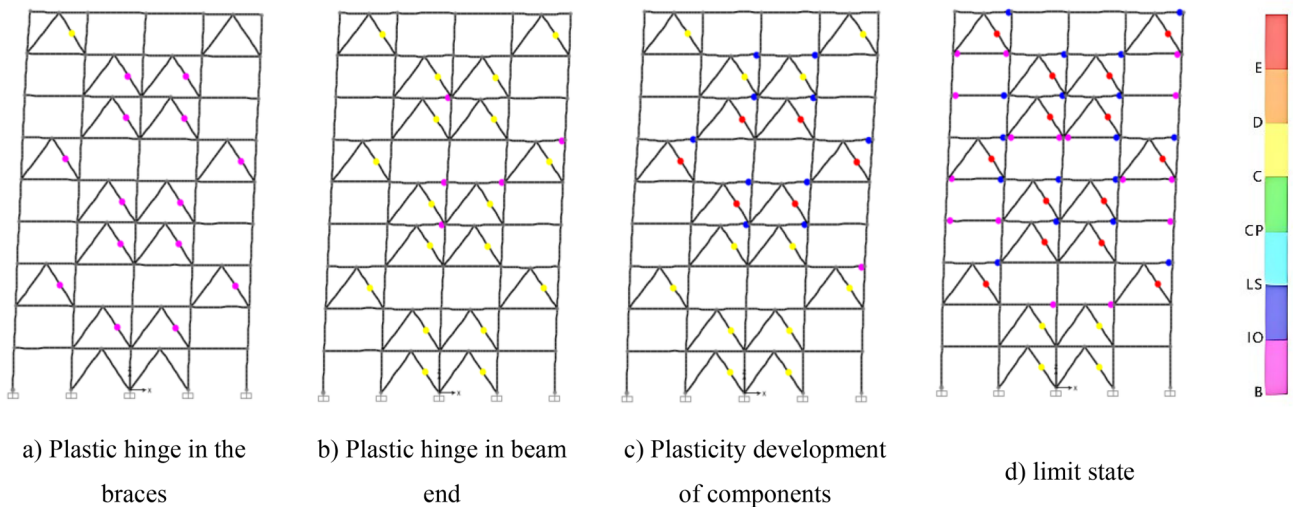
d) limit state

Fig. 27 Sequence and location of plastic hinge formation in braces of the optimized arrangement structure. **a** Plastic hinge in the braces, **b** Plastic hinge in beam end, **c** Plasticity development of components, **d** limit state

was to examine the elastic–plastic properties of the structure after optimization and assess the rationality of the yielding mechanism within the structural members. This process aimed to validate the reasonableness of the optimized brace arrangement.

4.2.1 Pushover analysis of four-span, nine-story center-braced steel frame

Four-span, nine-story structures with both traditional braced arrangement 1 and optimized braced arrangement 1, as

discussed in Sect. 4.1, were selected for the pushover analysis. The results are shown in Figs. 26 and 27.

In Fig. 26, an examination of the sequence of plastic hinge formation in the structure with the traditional brace arrangement reveals that plastic hinges initially manifested in the braces. As brace plasticity progressed, plastic hinges developed simultaneously in both the beams and columns. Subsequently, additional plastic hinges emerged in the other beams and secondary columns, ultimately resulting in the withdrawal of eight brace members. This sequence of plastic hinge appearances in the structure was deemed
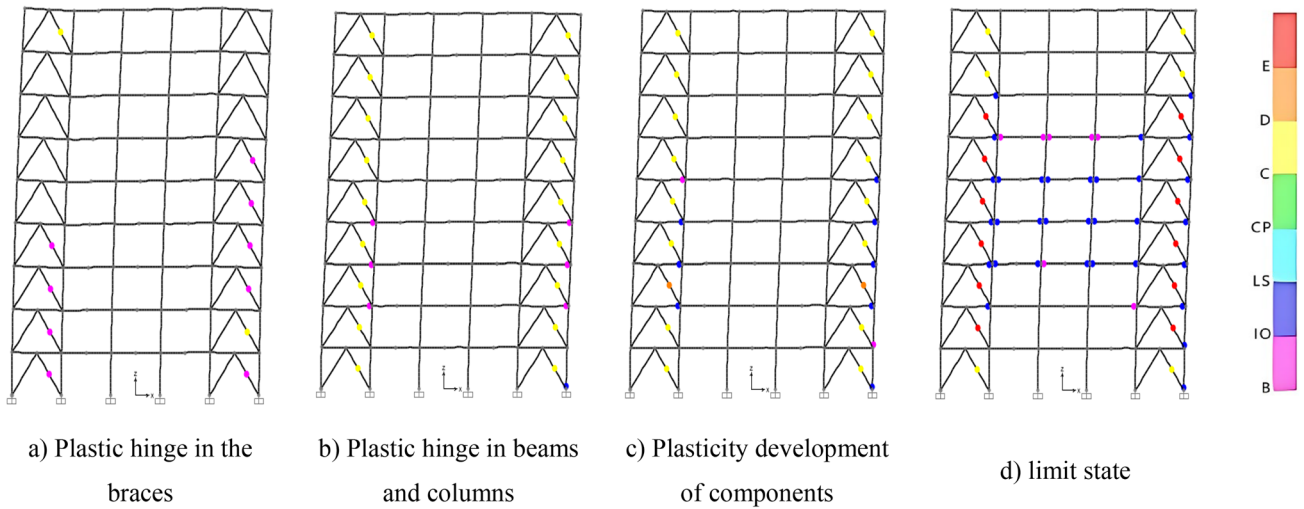
a) Plastic hinge in the   b) Plastic hinge in beams   c) Plasticity development   d) limit state
braces   and columns   of components

Fig. 28 Sequence and location of plastic hinge formation in braces of the traditional arrangement structure. **a** Plastic hinge in the braces, **b** Plastic hinge in beams and columns, **c** Plasticity development of components, **d** limit state

a) Plastic hinge in the   b) Plastic hinge in beam   c) Plasticity development   d) limit state
braces   end   of components
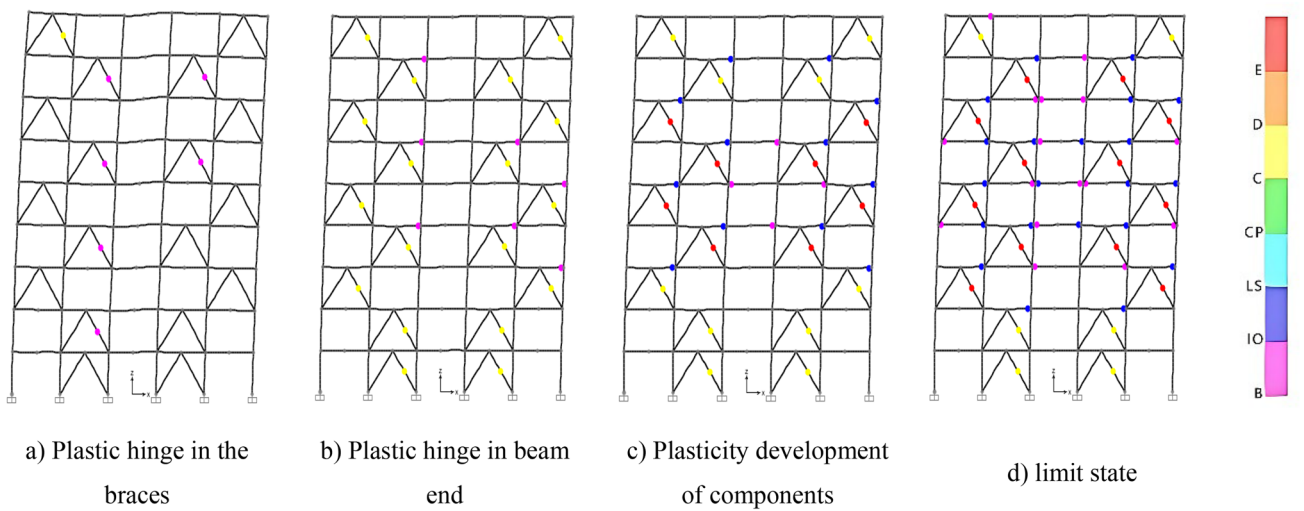
Fig. 29 Sequence and location of plastic hinge formation in braces of the optimized arrangement structure. **a** Plastic hinge in the braces, **b** Plastic hinge in beam end, **c** Plasticity development of components, **d** limit state

unreasonable because of the premature appearance of plastic hinges in the columns before the beams, which lacked a logical yielding mechanism. In contrast, for the structure with the optimized brace arrangement in Fig. 27, the plastic hinge sequence was as follows: plastic hinges emerging in a portion of the braces → plastic hinges manifesting in all braces → plastic hinges appearing in some beam ends → plastic hinges developing in the majority of beam ends, leading to the withdrawal of some braces until the final stage, where 14 braces withdrew. This formed a double lateral force-resisting structural system, representing an ideal yielding mechanism for the members.
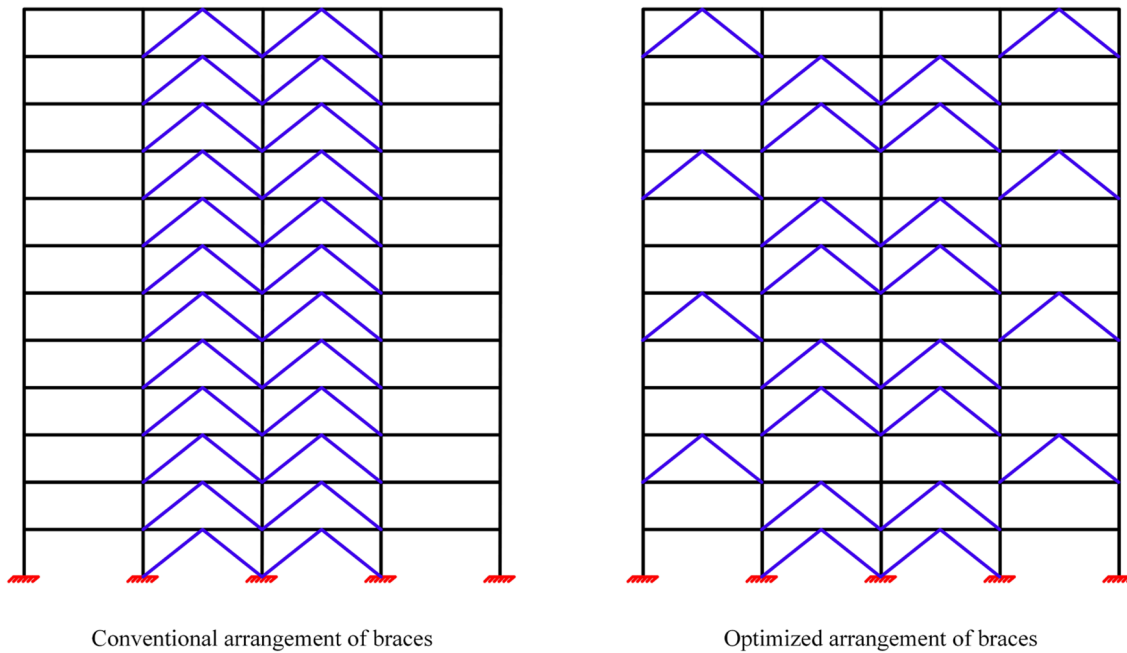
Conventional arrangement of braces   Optimized arrangement of braces

Fig. 30 Conventional and optimized arrangements of frame braces

4.2.2 Pushover analysis of five -span, nine-story center-braced steel frame

Structures with five-span, nine-story traditional braced arrangement 1, and optimized braced arrangement 1, as discussed in Sect. 4.1, were selected for the pushover analysis. The results are shown in Figs. 28 and 29.

In conjunction with Figs. 28 and 29, it is evident that the sequence of plastic hinge emergence in the five-span, nine-story structure mirrored that in the four-span, nine-story structure. The traditional bracing arrangement tended to induce premature plastic hinge formation in the columns, leading to an impractical yielding mechanism for the components. Conversely, the optimized bracing arrangement enhanced the sequence of plastic hinges, establishing a hinging sequence of brace→beam→column. This resulted in the formation of an efficient double lateral force-resisting structural system, showing an ideal yielding mechanism for the structure.

5 Dynamic time–history analysis of steel frame with optimized center brace arrangement

5.1 Basic information on structural modeling

The chosen structural model consisted of a twelve-story steel frame with four spans, featuring a double-brace arrangement on each floor. The brace arrangement was optimized

Table 5 Load information for each story in the steel framework

| Load type	Load size (kN/m)
Top floor constant load	40
Top floor live load	20
Standard layer constant load	30
Standard layer live load	18

in accordance with the principles outlined in Sect. 3, as shown in Fig. 30. Subsequently, the study delved into an in-depth exploration of the dynamic characteristics exhibited by the structure as a consequence of the optimized brace arrangement.

The structure had a height of 3.6 m and a column spacing of 7.2 m. It is located in an area characterized by an 8-degree (0.2 g) fortification intensity and is classified as a class II site. The seismic design group was a single group. Detailed information on the structural loads is presented in Table 5.

A finite element model of the structure was generated using SAP2000 software, with particular emphasis on evaluating the impact of brace arrangement positioning. The structural components were constructed using Q235 steel, with round steel pipes employed for the braces, and H-beams for the beams and columns. The nodes were connected using rigid connections. Detailed cross-sectional data of the members are presented in Table 6.

Table 6 Information on cross-sectional size of steel frame components

Layer number	Column section (mm)	Beam section (mm)	Brace section (mm)
1–3	400×400×21×21	450×200×9×14	100×10
3–6	400×400×18×18	450×200×8×12	100×10
6–9	400×400×18×18	450×200×8×12	100×10
9–12	400×400×15×15	400×200×7×11	100×10
12–15	400×400×15×15	400×200×7×11	100×10

Fig. 31 Time–history curve of seismic wave
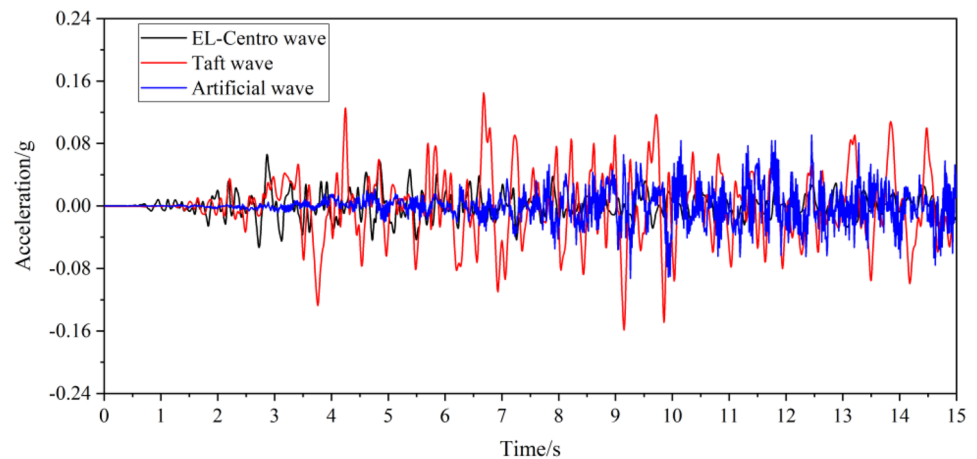
5.2 Seismic wave selection and adjustment

Based on the site category, fortification intensity, and design grouping of the structural model, we selected two representative strong earthquake seismic waves, specifically the El-Centro and Taft waves. Additionally, an artificial seismic wave was generated to conduct a time–history analysis of the aforementioned model. Seismic waveforms occurring within the first 15 s were selected for the analysis, accounting for both common and rare structural encounters. The acceleration–time curves for these three sets of seismic waves are shown in Fig. 31.

5.3 Structural time–history analysis under frequent earthquakes

The structure was subjected to three distinct seismic waves: an El-Centro, Taft, and artificial waves. Subsequently, we obtained the time–history responses for displacement, base shear, and maximum interlayer lateral displacement for both the traditional brace arrangement structure system and brace optimization arrangement structure system under frequent earthquake conditions, as depicted in Fig. 32.

Comparing the top lateral displacement responses of the structure under the optimized brace arrangement and the traditional brace arrangement in Fig. 32, it is evident that the displacement response of the structural system during the 8-degree frequent earthquake was notably smaller with

the optimized brace arrangement. Further analysis attributed this improvement to the optimized brace arrangement, which enhanced the structural force transmission path, resulting in an increased lateral stiffness of the structural system. This enhanced stiffness effectively reduced the structural displacement response during seismic events. Consequently, it is advisable to consider brace arrangement optimization in future projects as a means of enhancing structural performance and seismic resilience.

Under frequent earthquakes, both the optimized brace arrangement and traditional structural system exhibited base shear values that were closely aligned with the seismic design code. This alignment indicates that the disparity between the structural base shear corresponding to each time–history curve and the value calculated from the response spectrum was less than 35% of the calculated response spectrum value. Additionally, the difference was less than 20% of the calculated response spectrum value between the average base shear values derived from the time–history curves and calculated response spectrum values. The comparative results are presented in Tables 7 and 8, respectively. Hence, all three seismic waves adhere to the specified criteria and are suitable for dynamic time–history analysis of the aforementioned structure.

Figure 33 illustrates the inter-story lateral displacement observed in both the optimized and traditional brace arrangements during a multi-occurrence earthquake. Notably, the inter-story lateral displacement for both arrangements
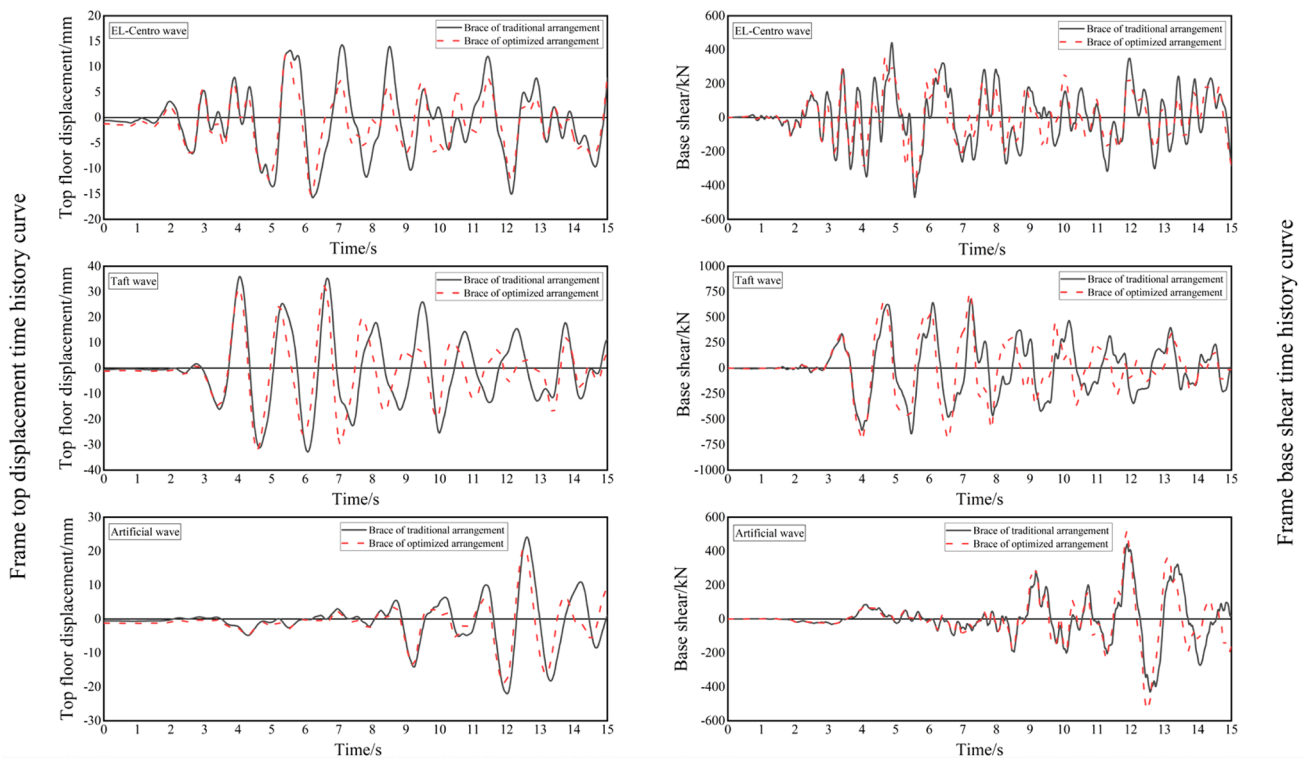
Fig. 32 Time–history curves of traditional and optimized arrangements of braces under frequent earthquakes

Table 7 Maximum base shear in traditional brace arrangements using time–history analysis and reaction spectrum methods

Seismic wave	Calculation by time–history analysis method maximum base shear	Calculation by reaction spectrum method base shear	Calculation ratio
El-Centro	470.39	606.74	22.47%
Taft	677.92	606.74	11.73%
Artificial wave	443.04	606.74	26.98%
Average value	530.45	606.74	12.57%

Table 8 Maximum base shear in optimized brace arrangements using time–history analysis and reaction spectrum methods

Seismic wave	Calculation by time–history analysis method maximum base shear	Calculation by reaction spectrum method base shear	Calculation ratio
El-Centro	411.76	612.52	33.78%
Taft	742.52	612.52	21.22%
Artificial wave	516.85	612.52	15.62%
Average value	557.04	612.52	9.06%

remained at approximately 5 mm. Moreover, the inter-story displacement angle remained below the elastic inter-story displacement angle threshold of 1/250. Upon closer examination, it becomes apparent that the average maximum inter-story lateral displacement in the optimized brace arrangement was slightly smaller than that in the traditional brace arrangement. This reduction can be attributed to the reinforcement of the structural floors achieved through the enhanced lateral stiffness resulting from the optimization of the brace arrangement. Consequently, specific areas within the structure experienced a decrease in inter-story lateral movement. This improvement is a direct outcome of the optimized brace arrangement, which bolsters the lateral stiffness of the structural floors and effectively mitigates the inter-story lateral displacement.
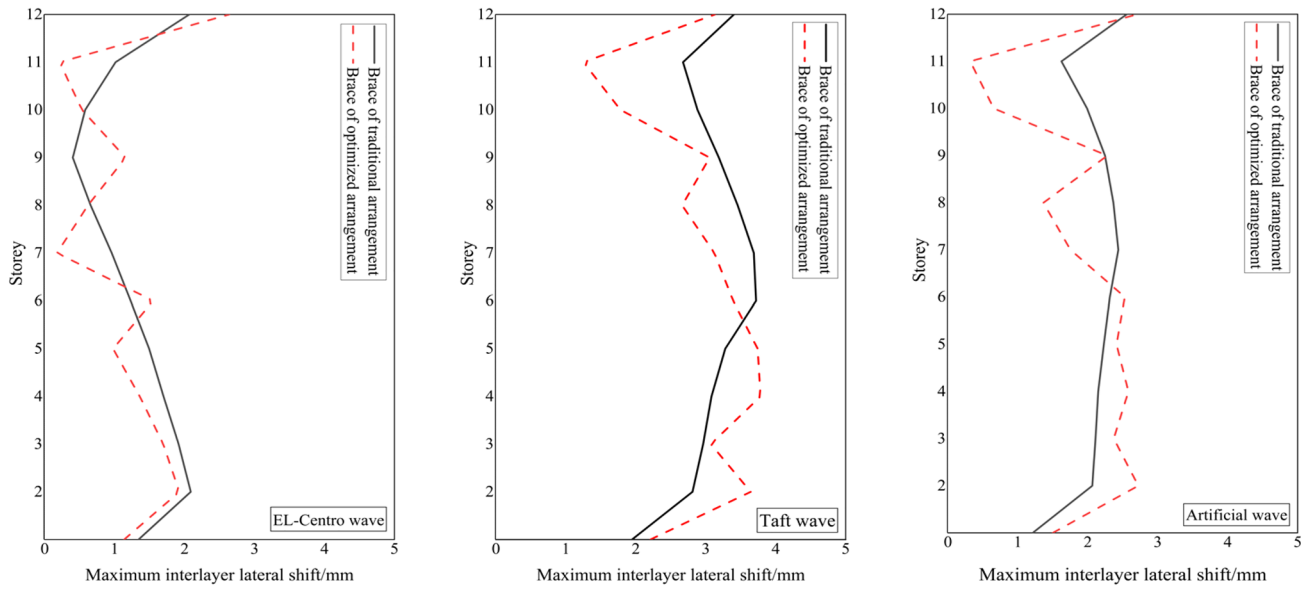
Fig. 33 Comparison of maximum lateral displacements under frequent earthquakes
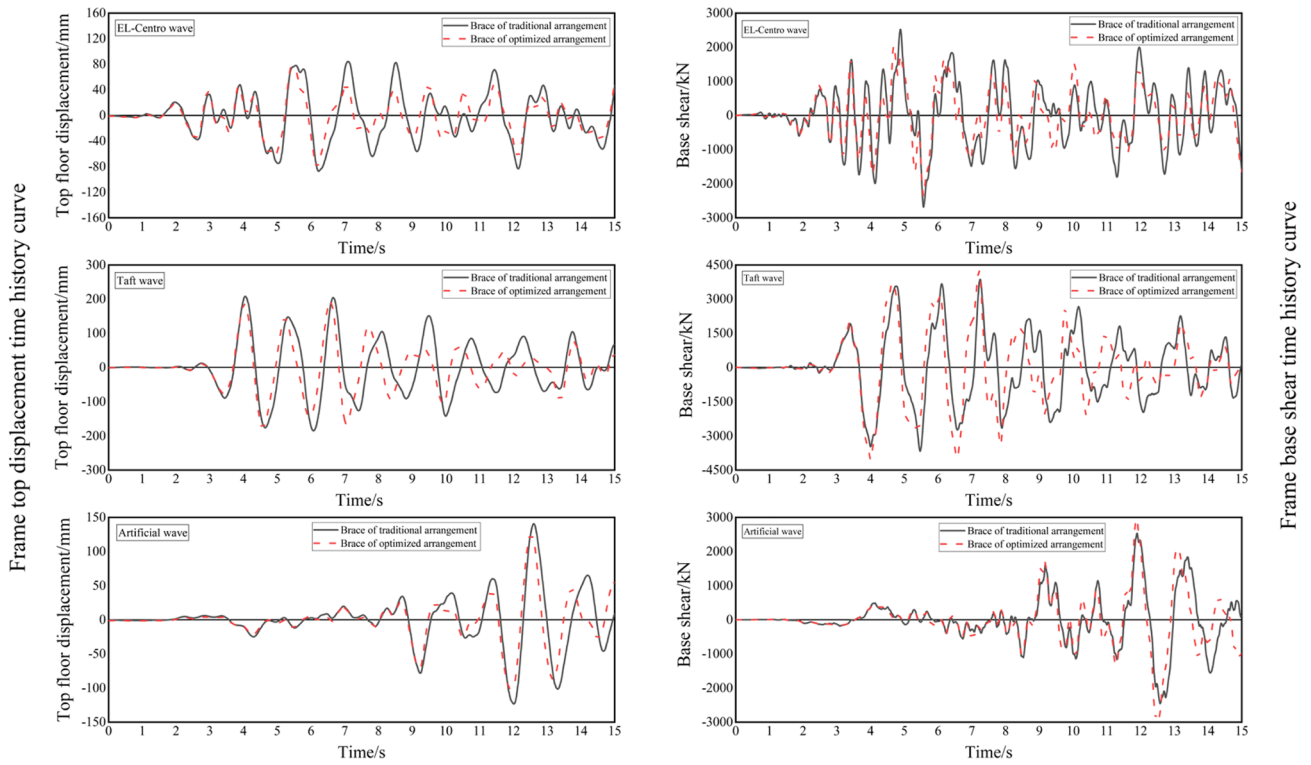

Fig. 34 Time–history curves of traditional and optimized arrangements of braces under rare earthquakes

5.4 Structural time–history analysis under rare earthquakes

The structure was subjected to three seismic waves: an

El-Centro wave, Taft wave, and artificial wave. Subsequently, the displacement, base shear time–history responses, and maximum interlayer lateral displacement of both the traditional brace arrangement structure system and
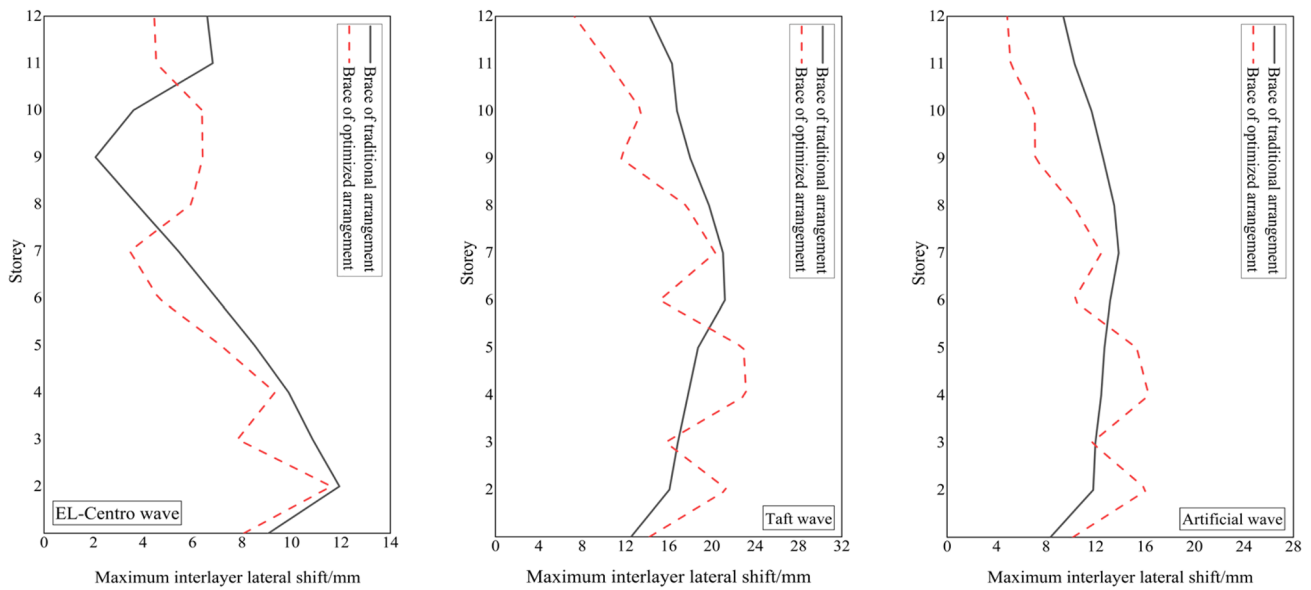
Fig. 35 Comparison of maximum lateral displacements under rare earthquakes

brace optimization arrangement structure system under rare earthquake conditions were recorded, as shown in Fig. 34.

Comparing the top lateral displacement responses of the structure under the optimized brace arrangement and the traditional brace arrangement in Fig. 34, it is evident that the optimized brace arrangement reduced the structural system's displacement response during rare 8-degree earthquakes. This seismic performance improvement is attributed to the repositioning of the brace distribution. It is recommended that optimized brace arrangements be incorporated following the established rules in future projects. Moreover, the base shear values for both the optimized and traditional brace arrangements remained similar under rare earthquake conditions.

Figure 35 depicts the inter-story lateral displacement profiles of the structure under the influence of three sets of rare earthquake seismic waves, considering different brace arrangement positions. Notably, both the traditional and optimized brace arrangements adhered to the specification requirements for inter-story lateral displacement. The inter-story lateral displacements in both arrangements exhibited similarity, with the mean value of inter-story lateral displacement being slightly smaller in the optimized brace arrangement than in the traditional arrangement.

6 Conclusions

This study focused on the optimization of conventional center brace steel frame structural systems, with a particular focus on the standard herringbone center brace steel frame. This investigation explored the relationship between the positioning of brace arrangements within a structure and its structural performance. A novel optimization approach was proposed for optimizing the brace plane layout in center brace steel frame structural systems. This method demonstrated the ability to optimize the structural brace arrangement efficiently and precisely, and explored the static and dynamic aspects of the mechanical behavior of the structure after the implementation of the optimal brace arrangement. To encapsulate the research findings outlined above, the primary conclusions are summarized as follows:

(1) A fundamental theoretical formula for calculating the equivalent lateral stiffness of frame stories with different brace span arrangements was established. The proposed theoretical analysis was sufficiently validated and verified for accuracy through a comparison with finite element simulation results.

(2) The impact of varied member stiffnesses on the overall lateral stiffness of the structure was examined, and the results indicated that the axial stiffness of members within the frame-braced structural system played a key role. Subsequently, a simplified theoretical model was introduced to facilitate the rapid assessment of the lateral stiffness of the structure with respect to the influence of the brace arrangement. Subsequently, the utili-

zation of a fundamental brace unit helped elucidate the brace optimization arrangement principles, leading to the proposal of a brace plane optimization arrangement.

(3) A comparative evaluation of the structural performance of the traditional and optimized brace arrangements was conducted. It is evident that the lateral displacement was significantly improved with the optimized brace arrangement, resulting in a more uniform and reduced internal force distribution among the structural members, which effectively strengthened the lateral stiffness of the structure. Notably, the traditional brace arrangement often subjected the bottom columns to substantial axial forces, whereas the optimized brace arrangement reduced the maximum axial force in the bottom column by more than 50%. Moreover, the traditional vertical through-span brace arrangement can induce premature plastic hinge development in columns, leading to an unfavorable member yielding mechanism. Conversely, the optimized brace arrangement established a desirable yielding mechanism, preventing plastic hinges at the column ends and forming an effective double lateral force-resisting structural system.

(4) In response to multiple and rare earthquakes, the dynamic structural response was notably reduced following the implementation of the optimized brace arrangement. This enhancement in seismic performance was attributed to the strategic adjustment of the brace arrangement positions. Consequently, it is advisable to incorporate the brace optimization method into construction projects to achieve cost-effectiveness and structural efficiency through the utilization of optimized brace arrangements.

In future research, we will assess the optimized arrangement of the center brace steel framing system using an enhanced optimization algorithm built upon the method proposed in this paper, with the total structure cost as the primary objective.

Author Contributions All authors have made significant contributions to the work reported in this manuscript. Specifically: Conception and Design: Yunyun Zhu and Jianrong Pan made substantial contributions to the conception and design of the work. Data Acquisition, Analysis, and Interpretation: Yunyun Zhu and Yanjing Fan were responsible for the acquisition, analysis, and interpretation of data. Software Development: Zhoupeng Wu and Fangxin Hu created new software used in the work. Drafting and Revising the Manuscript: Jianrong Pan and Zhan Wang drafted the work and revised it critically for important intellectual content. Approval of the Final Version: All authors have approved the final version of the manuscript to be published. Accountability: All authors agree to be accountable for all aspects of the work in ensuring that questions related to the accuracy or integrity of any part of the work are appropriately investigated and resolved.

Declarations

Competing interest The authors declare that there are no conflict of interest regarding the publication of this paper.

Replication of results A finite element numerical model with the original data is available in the Supplementary Materials. Tables 2, 3, 4, and 5 and Figs. 26, 27, 28, 29, 30, 32, 33, 34, and 35 show data from the optimization results.

References

Bochao F, Gao Y, Wang W (2022) Dual generative adversarial networks for automated component layout design of steel frame-brace structures. Autom Constr 146:104661. https://doi.org/10.1016/j.autcon.2022.104661

Chen L, Jin B (2011) Research on structural optimization method for aircraft bulkhead based on the path of force transfer. Adv Aeronaut Sci Eng 2(02):199–204

Chen M, Zhang G, Chengxin Y (2020) Research on the application of an information system in monitoring the dynamic deformation of a high-rise building. Math Probl Eng. https://doi.org/10.1155/2020/3714973

Fang C, Linzell DG (2021) Examining progressive collapse robustness of a high-rise reinforced concrete building. Eng Struct 248:113274. https://doi.org/10.1016/j.engstruct.2021.113274

Ghannadi P, Khatir S, Kourehli SS (2023) Finite element model updating and damage identification using semi-rigidly connected frame element and optimization procedure: an experimental validation. Structural 50:1173–1190. https://doi.org/10.1016/j.istruc.2023.02.008

Gray MG, Christopoulos C, Packer JA (2017) Design and full-scale testing of a cast steel yielding brace system in a braced frame. J Struct Eng 143:4. https://doi.org/10.1061/(asce)st.1943-541x.0001692

Hassanzadeh A, Gholizadeh S (2019) Collapse-performance-aided design optimization of steel concentrically braced frames. Eng Struct 197:109411. https://doi.org/10.1016/j.engstruct.2019.109411

Hongjia L, Gilbert M, Tyas A (2018) Theoretically optimal bracing for pre-existing building frames. Struct Multidisc Optim 58:677–686. https://doi.org/10.1007/s00158-018-1921-7

Imran M, Wang D, Wahab MA (2023) Three-dimensional finite element simulations of fretting wear in steel wires used in coal mine hoisting system. Adv Eng Softw 184:103499. https://doi.org/10.1016/j.advengsoft.2023.103499

Kontoni D-P, Farghaly AA (2023) Enhancing the earthquake resistance of RC and steel high-rise buildings by bracings, shear walls and TMDs considering SSI. Asian J Civ Eng 24:2595–2608. https://doi.org/10.1007/s42107-023-00666-6

Lim H, Seo J, Song D (2020) Interaction analysis of countermeasures for the stack effect in a high-rise office building. Build Environ 168:106530. https://doi.org/10.1016/j.buildenv.2019.106530

Ling Y, Ni J, Antonissen J (2022) Numerical prediction of microstructure and hardness for low carbon steel wire Arc

additive manufacturing components. Simul Model Pract Theory 122:102664. https://doi.org/10.1016/j.simpat.2022.102664

Mohammadi SA, Moghaddam A, Faroughi A (2015) The effect of number and position of braced frames on column behavior of the dual steel structural system (MRF and EBF) (With a view on amplified seismic load). Ciência e natura 37:277. https://doi.org/10.5902/2179460X20858

Mourhatch R, Krishnan S (2022) Performance quantification of tall steel braced frame buildings using rupture-to-rafters simulations. J Earthquake Eng 26:4105–4128. https://doi.org/10.1080/13632469.2020.1822232

Nie J (2016) The future of structural engineering in China—high-performance structural engineering. China Civil Eng J 49:1–8. https://doi.org/10.15951/j.tmgcxb.2016.09.001

Rahgozar N, Rahgozar N, Moghadam AS (2017) Probabilistic safety assessment of self-centering steel braced frame. Front Struct Civ Eng 12:163–182. https://doi.org/10.1007/s11709-017-0384-z

Stromberg LL, Beghini A, Baker WF (2022) Numerical evaluation on collapse-resistant performance of steel-braced concentric frames. J Constr Steel Res 193:107268. https://doi.org/10.1016/j.jcsr.2022.107268

Tan Z, Zhong W, Meng B (2022) Numerical evaluation on collapse-resistant performance of steel-braced concentric frames. J Constr Steel Res 193:107268. https://doi.org/10.1016/j.jcsr.2022.107268

Thai H-T, Ngo T, Uy B (2020a) A review on modular construction for high-rise buildings. Structures 28:1265–1290. https://doi.org/10.1016/j.istruc.2020.09.070

Thai H-T, Ho QV, Li W (2020b) Progressive collapse and robustness of modular high-rise buildings. Struct Infrastruct Eng 19:302–314. https://doi.org/10.1080/15732479.2021.1944226

Tianjian J (2003) Concepts for designing stiffer structures. Struct Eng 81:36–42

Tran-Ngoc H, Khatir S, Le-Xuan T (2022) Finite element model updating of a multispan bridge with a hybrid metaheuristic search algorithm using experimental data from wireless triaxial sensors. Eng Comput 38(3):1865–1883. https://doi.org/10.1007/s00366-021-01307-9

Türker T, Bayraktar A (2013) Finite element model calibration of steel frame buildings with and without brace. J Constr Steel Res 90:164–173. https://doi.org/10.1016/j.jcsr.2013.08.003

Wang X, Honglin Y, Chao L (2022) Seismic performance of new fabricated lightweight herringbone support seismic wall based on ZigBee sensor technology. Mob Inf Syst. https://doi.org/10.1155/2022/4235419

Xiaoye Y, Ji T, Zheng T (2015) Relationships between internal forces, bracing patterns and lateral stiffnesses of a simple frame. Eng Struct 89:147–161. https://doi.org/10.1016/j.engstruct.2015.01.030

Yang J, Qiang G, Wan H (2010) Research on pushover test of inverted-V concentrically braced steel frame. J Xi An Univ Archit Technol 45:656–662. https://doi.org/10.15986/j.1006-7930.2010.05.016

Zhang J, Zhao B, Ge J (2022) Numerical and experimental investigation on seismic behavior of the linked column steel braced frame system with energy-dissipating link beam at column base. J Build Eng 58:105002. https://doi.org/10.1016/j.jobe.2022.105002

Zheng L, Dou S, Zhang C (2023) Seismic performance of different chevron braced frames. J Constr Steel Res 200:107680. https://doi.org/10.1016/j.jcsr.2022.107680